NTNU
Innovation and Creativity

Characterization of medical piezoelectric ultrasound transducers using pulse echo methods.

Janani Mylvaganam

Master of Science in Electronics
Submission date: July 2007
Supervisor: Ilangko Balasingham, IET
Co-supervisor: Tonni Franke Johansen, ISB

Norwegian University of Science and Technology
Department of Electronics and Telecommunications

Problem Description

New methods for estimating ultrasonic transducer parameters are under development at the MR ultrasound group, Department of Circulation and Medical Imaging. The parameters are complex and their estimates will enable the designer to incorporate measured transducer parameters in improving the modeling of the ultrasound system.

Tasks:

- Find improved reflectors for pulse echo measurements
- Develop a reliable and repeatable experimental set up for pulse echo measurements using an ultrasound array
- Design and develop a method for transducer alignment with respect to the reflector
- Evaluate estimation schemes for complex transducer parameters including variation of:
  - pulse
  - filters
  - elimination of propagation delay
- Implement a simple uncertainty budget for the above estimations.

Assignment given: 26. January 2007
Supervisor: Ilangko Balasingham, IET

Abstract

In this thesis, a measurement set-up has been developed to characterize high frequency medical ultrasound transducers using a pulse echo set-up. This work is a continuation of an earlier project. The aim of this project is to improve the instrumentation to get more reliable, repeatable and consistent results. The transducer used in this project was a 20MHz annular array transducer with 8 elements. Parameters such as the electroacoustic transfer function and reflection coefficients of element 1 and 2 have been found for a sinusoidal burst excitation and a Gaussian excitation, to give examples for the estimation of these parameters. Developing the right instrumentation for the pulse echo set-up and transducer for pulse echo measurements has been emphasised, where a transducer holder and reflector have been constructed for characterization of elements 1-5. A cylindrical water resistant reflector with a curved top was designed giving certain degrees of freedom as opposed to the pure spherical reflector concerning positioning of the reflector with respect to the transducer. A slanted bottom was included in the design of the reflector causing reflections from the bottom to diffract and thus stopping these from interfering with the reflections of interest happening at the top of the reflector surface. A transducer holder was also designed and custom made for the transducer used in the project, where both mechanical and electrical considerations have been taken, as the holder makes alignment of the transducer with respect to the reflector easier and coaxial cables have been introduced to get more control over the signals going to and from the transducer array. Coaxial cables were chosen as these are easy to model, and have clear specifications in addition to having the property of shielding noise signals. Alignment of the transducer has been emphasised to make radiation into the focus of the reflector easier, although the design of the reflector also allows the reflector to be tilted in the allocation of its focus point. By taking detailed lateral scans of echoes received by the transducer using a robot, in addition to varying the distance between the transducer and the reflector with an increment of 0.2 mm, the reflection coefficients were found to be very sensitive to lateral positioning, and to some extent sensitive to axial positioning of the transducer with respect to the reflector. The elimination of propagation delay due to the signals travel in waterpath and electrical transmission and reception chain leading to the transducer ports has also been compensated for, as these delays will effect the complex values of the transfer function. The electrical propagation delay is eliminated by using a simulation program, and analysis of the time between two consecutive echoes is done in order to find the physical time delay in the water path the pulses travelled. The electro acoustic transfer function has also been found for element 1 and element 2, but with a much greater time delay than what was expected. An uncertainty budget of the obtained parameters has also been done to see the impact of laboratory equipment on the meaurements. Estimation schemes to obtain reflection coefficients and the electro acoustic transfer function have been developed, which are repeatable for further characterization for the whole transducer array. Existing MATLAB codes have been modified in simulations and some new codes have been written for analyzing measurement based estimation of transfer functions, reflection coefficients and effects of various filters on their characteristics. Different types of filters have been used on the recorded echo signals to eliminate noise from the estimated reflection coefficients. A better

control of the parasitic inductances due to the non coaxial cables in the system should perhaps be evaluated, and for further characterization of the transducer, the mechanical admittance can also be found by using the estimated reflection coefficients and electro acoustic transfer function.

Preface

This report is the result of a project under The Department of Electronics and Telecommunications at NTNU, based on theoretical and practical work performed during the spring semester 2007. This work done is a continuation of a similar work commenced in autumn of 2006 and has given me increased insight in practical ultrasonic imaging and aspects of design and construction of ultrasonic transducers having the opportunity to work with hardware and software related to ultrasonic imaging applications. The work was done under the supervision of dr.ing Tonni F. Johansen at the Department of Circulation and Medical Imaging at NTNU. I would like to thank him for all the valuable discussions with him and all his guidance throughout the project. Engineers Arnfinn Sira and Ketil Jensen have been of timely and great help with the practical aspects of the project. PhD student Øyvind Standal has also made his time available for me in conjunction with the laboratory work. I would like to thank them all for their kind help and supervision. It has all in all been very interesting work, giving me further insight into transducer characterization problems and the usage of equipment related to medical ultrasonics.

Janani Mylvaganam 05.07.2007 Trondheim,

Contents

List of Symbols

λ - wavelength [m]

c - sound speed [m/s]

f - frequency [Hz]

ρ - mass density [kg/m$^-$3]

Z - specific acoustic impedance [kg/m^{2}s][Rayl]

u - vibration velocity [m/s]

p - particle pressure [Pa]

r - radial distance in spherical coordinates [m]

t - time [s]

k - wavenumber [1/m]

ω - angular frequency, also known as $\omega = 2\pi f$, [s^{-1}]

R - general reflection coefficient

T - general transmission coefficient

$I(r)$ - intensity of a plane wave [W/m^2]

$\mu(f)$ - intensity absorbtion coefficent as a function of frequency [1/m]

k_d - amplitude absorbtion coefficient

C - absorbtion constant in [Np/cm]

L - thickness of piezo electric plate [m]

$V_r(\omega)$ - signal out of receiver amplifier at transducer output [V]

Z_L - load impedance of transducer [Ω]

$H_{tt}(\omega)$ - transmitting transfer function

$R_{T,n,m}$ - reflection coefficient for the setup in this thesis where n, m are the echo numbers

I - current [A]

V - voltage [V]

Y_m - admittance [S]

C' - capacitance [F]

R' - resistance [$mega$]

L' - inductance [H]

τ_{echo} - time lag between to consecutive echoes [s]

τ_v - time lag and phase due to the water [s]

d_{echo} - distance between two consecutive echoes [m]

m - "Wiener filter" constant

$V_{tt,m}$ - measured V_{tt} [V]

V_{r1m} - first echo, measured [V]

V_{r1} - first echo [V]

u_x - uncertainty associated with measurement/estimated value of parameter x

α - constant for filter selection

List of Tables

List of Figures

Chapter 1

Introduction

1.1 Background

Ultrasound imaging is very popular because it is considered reliable, simple, cheap and nearly free of risk in comparison to other imaging techniques. The transducer is the most important component of any ultrasound imaging system, converting electrical energy into mechanical energy in the form of vibrations in transmission mode and converting mechanical energy back to electrical energy during receiving mode. The transducer, in many applications, is excited with a variety of transients or impulses. In many practical cases, the specifications and properties of the transducers are unknown. The characteristics of a transducer is what utimately determines the image quality. Pulse echo imaging and the analysis of the transmitted pulses and the echoes from a known target is a useful way to obtain information characterizing the transducer. Reflection coefficients, electroacoustic transfer functions, terminated/open circuit insertion losses and the transducer efficiency are examples of parameters commonly used to characterize the transducer. These parameters are determined by analysis of the transmitted pulses and the recieved echoes, when the equivalent electrical input impedance and the electrical termination of the transducer are known.

1.2 Applications of High Frequency Ultrasonic Transducers

The first transducers suitable for high frequency clinical imaging (30-100 MHz) were developed in the 1980's, providing images of subsurface structures with microscopic resolution. Most applications of high frequency ultrasound are therefore for surfaces, as the high frequencies increase the resolution, but get attenuated more, so penetration decreases, as seen in Figure 1.1, where the resolution for transducers with a range of f-numbers [1] and the penetration are both given for a range of frequencies. The penetration is given to be 0.5 dB/(cm $\text{MHz}^{1/2}$) in tissues [7]. Medical applications of high frequency ultrasound include eye imaging, catheter based intravascular imaging, intra-articular imaging and *in vivo* imaging of mouse embryonic development. Some examples of such clinical applications of high frequency ultrasound are described briefly below. Further information about medical and biological applications of high frequency ultrasound can be found in [13] and [7].

[1] The f-number is given as f =focal distance/diameter

1.2.1 Imaging Anterior Segment of the Eye

The anterior segments of the eye shown schematically in Figure 1.2 can be imaged very well by ultrasound backscatter microscopy (UBM), as structures of clinical importance lie in the range of the high frequency beam coming from the UBM. Ultrasound backscatter microscopy is an extension of the B-mode ultrasound backscatter methods, though operating at higher frequencies. In Figure 1.2 the ultrasonic image of an excised eye is shown. This image shows the anterior segments of the eye at 50 MHz and was obtained by using a prototype ultrasonic backscatter microscope [2] developed at the University of Southern California [21]. Special areas of importance are the ciliary and zonules, as these areas are prone to cyst and tumor growth. The area where the iris and cornea join is important as this is where glaucoma starts. Examples of transducer configurations used for such opthalmic studies are shown in Figure 1.3, where frequency ranges of 50-80 MHz and f numbers ranging from 1.1 to 2.2 have been used.

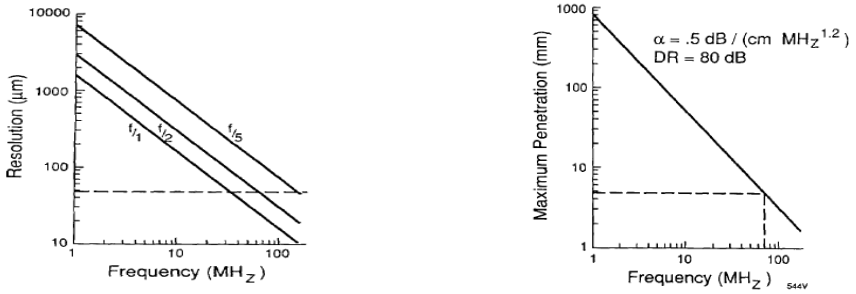

(a) Resolution as a function of Frequency (b) Penetration as a function of frequency

Figure 1.1: Resolution and penetration varying with frequency

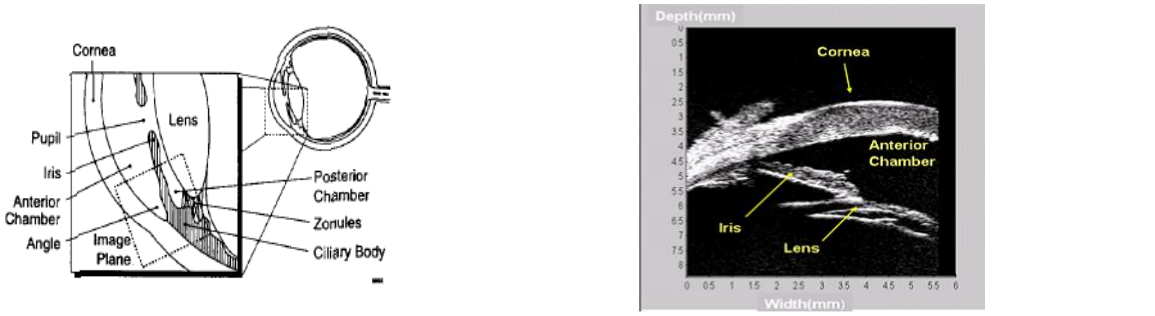

(a) Anterior chamber of the eye, [7] (b) Image of the excised eye at 50 MHz using a UBM, [21]

Figure 1.2: Structures within anterior chamber (a), Ultrasonic eye imaging (b)

1.2.2 Intravascular Imaging

Intravascular ultrasound is a currently available technique that provides real time cross- sectional images of coronary arteries *in vivo*. Rotating single element catheters with center frequencies 30 or 40 MHz are currently used for clinical purposes [9], an important application being improved diagnosis of the diseased coronary artery. Below in Figure 1.4, the cross sections of a rabbit aorta *in vivo* using intravascular ultrasound tissue harmonic imaging is shown.

[2] The Ultrasonic Backscatter Microscope system has same component blocks as a conventional B-mode imaging system, but the operating frequency is an order of magnitude higher, [7]

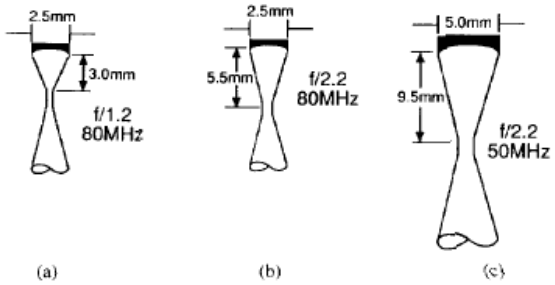

Figure 1.3: Transducers used in opthalmic imaging, [7]

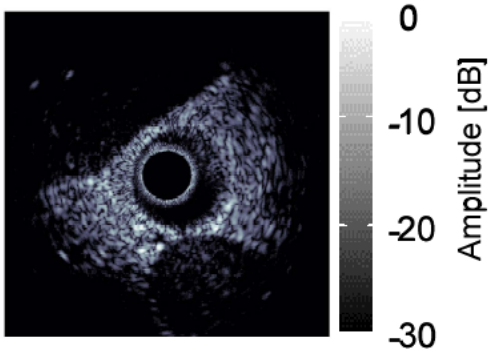

Figure 1.4: Cross-section of an atherosclerotic [3] rabbit aorta in vivo, [9]

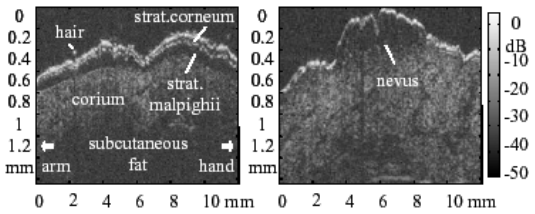

Figure 1.5: B-mode images at 100 MHz, left: healthy skin at wrist transition, right: nevus at the forearm, [8].

1.2.3 Skin Imaging

High frequency ultrasound in the range 20MHz has become a standard in skin imaging, and imaging of the upper layers of the skin [4] is of medical interest, as this can give valuable information about skin diseases. For this purpose, higher frequencies such as 100 MHz is desirable, as 20 MHz gives restrictions in spacial resolution due to limitations in bandwidth and center frequency [8]. The images of skin with and without a nevus [5] is shown in Figure 1.5.

1.2.4 Non Medical Applications

High frequency ultrasound transducers are also used in non-destructive testing (NDT), for detecting miniscule flaws on pipes and structures. Here the high frequency transducers can be used for high resolution ultrasonic imaging of materials like microelectronic components and ceramic parts, where an axial resolution better than 0.025 mm can be achieved in some cases. Thickness gaging of very thin nonmetallic coatings on nonmetallic substrates, like paint on plastic, and measuring individual layers of multilayer coatings are also examples of such applications. In addition, high frequency ultrasonics is also used in material analysis, such as in thickness gaging of very small polymer tubing with very thin wall thickness, for example medical catheters [13].

1.3 Limitations with High Frequency Ultrasound

With applications in ultrasound changing from low frequency to high frequency, the design of system hardware to provide reliable operations will become a challenge for the electronic and system designer. For example, noise tolerance should be stricter, due to the increased attenuation at higher frequencies [5].

1.4 Motivation for this Thesis

There are many reasons for characterizing and testing ultrasonic transducers. It is important to ensure that a suitable transducer is selected to perform a given task, especially in NDT applications. The transducers' performance should also meet the expectations given on the data sheet from the company or specified by the user. It is common that transducer performances deviate from its specifications. Transducer characterization is also important when analyzing

[4] also called epidermis
[5] nevus is a skin disease

the transducer's effect on the ultrasound signal, especially when signal processing and analysis are going to be performed. In order to obtain transducers with consistent and predictable performances, it is important that the supplier of the transducer is provided with the required specifications that deal with all significant design and performance characteristics. Even so, incoming transducers should be inspected to see whether they fulfill the purchase specifications.

A benefit of transducer characterization is the on-site assurance that the transducer's performance is as expected. One cannot assume that transducers of similar size, frequency, model and type produce equivalent results. They can in fact have very differing performances. It is important to measure transducer performance periodically throughout its life, as transducer elements tend to degrade in performance with usage and time. In fact an inspection procedure can become invalid if an appropriate routine is not tried and executed to remove or adjust for transducer deterioration. The transducers' effect on significant parameters of the ultrasound signal can also be accounted for through transducer characterization, especially when signal processing is to be performed, and uncommon signal parameters are being measured [23].

In this thesis, the reflection coefficient and the electro-acoustic transfer function of the transducer is determined in order to characterize the transducer. The electro-acoustic transfer function gives the direct relationship between the amplitude of the pressure wave hitting the transducer surface and the amplitude of the current wave generated in the piezoelectric element in the transducer due to surface vibrations caused by the pressure wave. The electro-acoustic transfer function is used to determine the transfer efficiency which describes how the reflection level is, according to the noise level of the electrical transmission chain. When sending an acoustic pressure wave (transmission beam) with the highest possible amplitude into a reflector, the signal will generate acoustic noise produced by the transmit beam itself in the target. Noise from the side lobes will be generated and added to the received signal, which are results of reflections from structures outside the observed region of the reflector. Acoustic noise will also be generated due to multiple reflections from structures within the region of interest around the reflector. In addition to this, the reflected wave will only be partially reflected from the transducer surface, when it is received. The reflection of the backscattered wave is described by the reflection coefficient.

Pulse echo measurements with a reflector are considered to be a good and simple way to obtain the reflection coefficent and the electro-acoustic tansfer function. There have been other methods before in order to characterize transducers, but as these involve using hydrophones and several transducers involving a complex set-up, pulse echo measurements are the prefered alternative, as it is also chosen in this thesis.

The mechanical positioning of the transducer with respect to the reflector is very important, in order to get the proper and undistorted pulses and echoes. Inaccurate positioning can lead to added energy loss due to diffraction in the transmitted pulses due to loss of directivity. This is a challenge in reflector measurements as it is vital that the transducer is positioned so that the transmitted pulses hit the focus point of the reflector and thus avoiding multiple reflections and reverberation effects. This requires that there is a stable mechanical fixture for the transducer so that there is a certain amount of control over the actual positioning of the transducer with respect to the reflector can be exercised.

The reflection coefficient and electro-acoustic transfer function are, in addition to the electrical impedance, parameters that describe the electro-acoustical behaviour of the transducer. By knowing these two parameters, one can introduce components with the transducer and make a software to calculate how the added components will affect the system. By determining the reflection coefficient and the electro acoustic transfer function together with the electrical impedance at the transducer ports, all the components in the the transducer's multiport structure matrix can be found, and by knowing the reflection coefficients and electro acoustic transfer function, the mechanical admittance at the transducer ports can also be found. In addition to this, the reflection coefficients can reveal to a certain extent whether

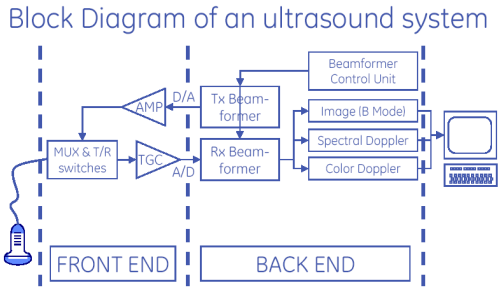

Figure 1.6: An overview of a typical ultrasound system, [14]

or not the transducer is radiating into the focus of the reflector. By ultimately characterizing an ultrasound array by finding the various parameters mentioned above, including bandwidth, directivity measurements and cross coupling effects [6] the ultrasound array can then be integrated in a probe housing and be interfaced into an ultrasound system. An example of such an ultrasound system is shown below in Figure 1.6.

1.5 Previous work in Transducer Characterization

There have been some previous work characterizing transducers, where different parameters have been found. L.Medino *et al.* [17] have studied the spatial and temporal characteristics of the acoustical pressure field generated by pulsed ultrasonic transducers under different boundary conditions. These parameters were determined both experimentally and numerically, where the simulations were performed using the temporal convolution between the numerical derivative of the impulse response and the longitudinal wave velocity with rigid and soft baffles as boundary conditions. T.P Lerch *et al.* [25] used an ultrasonic measurement model approach to determine the probe's effective radius, effective focal length and system efficiency factor. This was done by modeling both the transducer and the measurement system, where the whole measurement model process was expressed theoretically in the model. They used a simple measurement system with a spherical reflector [25]. P.G Kenny *et al.* [23] characterized an ultrasonic transducer by measuring the beam image, as this gives information about beam parameters as the propagation direction, beam diameter, divergence and cross sectional uniformity. They also measured the transducer electrical impedance, as this provides information about the structure of the transducer and the impedance matching between the transducer and the pulser/receiver. The insertion loss, which is a relative measure of the power conversion at a given frequency, was also found. The transducer impulse response was also found, which is a measure of the transducer sensitivity and flaw resolving capability. Most of their tests were performed using the pulse echo technique, similar to the method used in this thesis [23].

E. Lacaze *et al.* did work on characterizing a 20MHz ultrasound array and implementing it into a medical ultrasound system. The reason a 20MHz transducer was used was because this particular frequency gave an interesting combination of penetration or sensitivity and the expected image resolution. Electro acoustic characterization was performed on the full 128 element array, and in addition to this, the bandwidth, insertion loss and crosscoupling was also found. Finally the array was implemented in a medical ultrasound system after being

[6] crosscoupling is a disadvantagous effect that can occur in ultrasound arrays, in form of crosstalk between the array elements.

integrated into a probe housing. [6].

A recent study in transducer characterization was done by A.L. Lopéz Sánchez and L.W. Schmerr Jr. [24] where they determined both the transducer's sensitivity and impedance in a pulse echo set-up. They used a new model based approach to determine these parameters and at the same time compensating for cabling effects in the measurements, as these are significant at high frequencies. Considering the transducer as a linear, reciprocal device, the acoustical and electrical parameters are related through a 2 x 2 transfer matrix. A component of this matrix is the electro-acoustical transfer function. In principle, the elements of the transfer matrix can be obtained by taking a series of electrical and acoustic measurements at the transducer ports, but no such practical procedures currently exist that allows one to completely characterize a transducer in this manner. Therefore, A.L Lopéz Sánchez and L.W. Schmerr Jr. used the electrical impedance (obtained easily with an impedance analyzer) and a sensitivity in addition to an acoustic radiation impedance to account completely for the effects that an ultrasonic transducer has on an ultrasonic measurement system, when it acts either as a transmitter, or as a receiver.[24].

This thesis has used a similar set-up to that of S. Fath [10] for experimentally estimating the electro-acoustic transfer parameters as the reflection coefficient and the electro acoustic transfer function for piezoelectric ultrasound transducers. These are the same parameters determined in this thesis. Fath found that the existing setup used in his work was in some ways crude, and emphasised the importance of finding a better way to align the transducer with respect to the reflector with his existing experimental set-up. This thesis focuses on implementing an improvemed design of the measurement set-up. Using this set-up, the electroacoustic transfer function and the reflection coefficients are determined.

1.6 Outline

The first part of this report consists of theoretical principals and equations relevant to this project. Basic linear acoustic principles, pulse echo theory and theory concerning piezoelectric transducers are described briefly. The second part of this report covers the practical part of the project, where simulations, measurement set-up and results are described and discussed. Chapter 2 treats the general acoustic theory this project is based upon. Reflection and transmission principles during normal incidence, and pulse echo theory is covered briefly. Chapter 3 treats the general theory concerning ultrasonic transducers. Modeling of the transducer and the transceiver system is covered briefly, to give a general idea of how the transducer works. The Simulations done for this project and the transmission and receiver chain models used to compensate for the electrical path leading to the transducer electrodes are explained in Chapter 4. Simulations of what can be expected of the electro acoustic transfer function and the reflection coefficients are also included in order to give a general idea of what is to be expected in the results. Chapter 5 gives an overview of the instrumentation and measurement set-up used for the practical part of this thesis. As a major part of the instrumentation used was designed and therefore was an important part of the results of the project, this chapter also covers preliminary results needed to establish the main results, which are treated in Chapter 6. This chapter presents the reflection coefficients and the electro acoustical transfer functions found for the different pulses and the elements. Chapter 7 discusses the results, where an error analysis is taken on the main results of this work. Finally the conclusion gives the main results and observations of this project, hence suggesting further work that can be done on transducer characterization.

Chapter 2

Reflection and Transmission of Ultrasonic Waves

2.1 Acoustic Waves

Acoustic waves can either be described as shear waves, or compression waves, depending on how the particle movement is directed according to the wave propagation. If the particle movement is directed parallell to the wave propagation, the wave is a compression wave, also known as a longitudinal wave. If the particle movement is directed perpendicular to the wave propagation, the wave is a shear wave, also known as a transverse wave. With a plane compressed wave, the medium the wave propagates in is compressed and decompressed with a certain frequency, causing a pressure wave. The distance between two neighboring pressure maxima is given by the wavelength, λ. The wavelength is given by the simple relationship between displacement, speed and frequency, as

$$\lambda = c/f \tag{2.1}$$

Where c is the sound speed and f is the frequency.

The characteristic or acoustic impedance of the medium Z is then given as

$$Z = \rho c \tag{2.2}$$

Where ρ is the density of the medium.

2.1.1 Reflection and Transmission

When an acoustic wave hits a layer between two media with different acoustical properties, part of the wave will be reflected and part of the wave will be transmitted. The degree of reflection and transmission is dependent on the properties of the materials at the interface. There are two important boundary conditions that should be satisfied at all times when treating waves at an interface, and these are continuity of pressure and continuity of the normal component of the particle velocity. The incoming wave with a normal incidence is shown in Figure 2.1.

Conditions of continuity at the boundary yields the following equation for the pressure $\mathbf{p}$ and the normal component of the particle velocity, $\mathbf{u}$

$$\mathbf{p}_i + \mathbf{p}_r = \mathbf{p}_t \tag{2.3}$$

$$\mathbf{u}_i + \mathbf{u}_r = \mathbf{u}_t \tag{2.4}$$

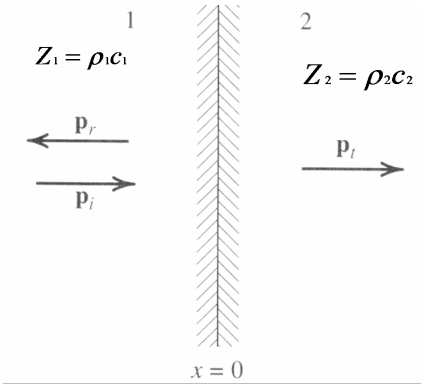

Figure 2.1: Normally incident wave at the boundary between two media, [16]

Where $\mathbf{p_i}$ is the incident wave traveling in the $+x$ direction and $\mathbf{p_r}$ is the reflected wave traveling in the $-x$ direction. Likewise, for $\mathbf{u_i}$ and $\mathbf{u_r}$. Division of (2.3) by (2.4) is a statement of the continuity of the normal specific acoustic impedance across the boundary, Z_1 and Z_2 in medium 1 and medium 2 respectively, illustrated in Figure 2.1. For a plane wave, $\mathbf{p}/\mathbf{u} = \pm Z$, resulting in the reflection coefficient R given in the equation below.

$$\mathbf{R} = \frac{Z_2 - Z_1}{Z_2 + Z_1} \tag{2.5}$$

Similarly the transmission coefficient T is given as

$$\mathbf{T} = 1 + \mathbf{R} = \frac{2Z_2}{Z_2 + Z_1} \tag{2.6}$$

2.1.2 Ultrasonic Attenuation

Attenuation is affected by many variables and it's generally hard to give exact values of the attenuation that can later be used for qualitative analysis. However, attenuation can often be obtained experimentally for a given material [26]. Ultrasonic attenuation is usually frequency dependent, and proportional to the depth of the wave propagation. As an ultrasound travels through tissue the wave intensity is attenuated due to three main factors [2],

Power absorption The absorption of wave energy to heat, this usually causes the strongest attenuation

Scattering Losses - The wave gets reflected and scattered, and thus it gets attenuated. Less than 10 percent of the attenuation is due to this form of attenuation

Geometric spread - Attenuation due to diverging regions of the beam.

The absorption attenuation of the intensity of a plane wave is modeled to be [10]

$$I(r) = I_0 e^{-\mu(f)r} \tag{2.7}$$

Where I_0 is the intensity of the incident wave, $I(r)$ is the intensity at a depth r, and $\mu(f)$ is the intensity absorption coefficient, and is as mentioned earlier, frequency dependent. Similarly, the attenuation of the pressure is found to be

$$p(r) = p_0 e^{-k_a(f)r} \tag{2.8}$$

Where p_0 is the pressure of the incident wave and k_d is the amplitude absorption coefficient. With the intensity being the pressure squared, we get that

$$\mu(f) = 2k_d(f) \tag{2.9}$$

In the range 1-10 MHz, the absorption coefficient follows a power law in frequency given as

$$\mu(f) = C(f(f_1)^m = C(\omega/\omega_1)^m \tag{2.10}$$

Where C is a constant with the unit [Np/cm]. For the relationship I_0/I it is common to use the decibel unit, dB given as

$$dB_{att} = r^{-1}10\lg I_0/I(r) = r^{-1}20\lg p_0/p(r) \tag{2.11}$$

2.2 Pulse Echo System

"A pulse echo system is any system that uses the scattering of electromagnetic waves (electrical or acoustic) from an object to obtain information about that object, "[22]. In other words pulse echo based measurement is a technique in which an ultrasonic transducer in transmission mode, emits a high frequency acoustic pulse into an object or medium. The pulse is reflected back to the same transducer operating in reception mode, [27]. In pulse echo imaging, a single transducer is therefore used to transmit an acoustic pulse and later recieve acoustic echoes. An example of this is A-mode imaging [1].

Important physical principles in pulse echo imaging such as reflection, transmission and attenuation have already been mentioned.

As mentioned earlier in this chapter, pulse echo imaging is often used to obtain information about materials or objects the waves propagate in, by analyzing the echoes and the initial wave. The objects mainly investigated in medical ultrasonic pulse-echo techniques can be described in two different ways:

Geometrical information Mapping of major structural boundaries as organ and tumor outlines by measuring the range of echoes generated at interfaces which usually are strong reflectors.

Physical information Observing changes in the image due to adjustments of the scanner controls

In order to extract physical information, one can either analyze the features of a single echo, or several echoes. When analyzing a single echo, its shape and amplitude can be used to characterize properties of the reflecting interface. When analysing several echoes, their amplitudes and spectra of signal wave numbers are evaluated over a region of tissues to provide criterias for tissue characterization. If however the reflectors characteristics are known, both physically and geometrically, characteristics about the transducer itself can be obtained by analysing the pulse and echoes from the given reflector [12].

By analyzing the bands of the pulses and the echoes, useful information about the signal energy in for different frequencies can be determined. The distribution of frequencies in the signals can also be analyzed by looking at the frequency spectra of the signals. In amplitude spectrum analysis, the fundamental frequency and its harmonics are observed as the freqency where the largest amplitude peak can be found. To obtain the fundamental frequency, the first largest amplitude can be found and its corresponding frequency, or the distance between two harmonics can be measured.

[1] A mode imaging is done by transmitting an ultrasonic pulse into an object and then recieving the backscattered signal with the same transducer

Chapter 3

Ultrasonic Transceiver System

3.1 General Qualities

The high frequency medical ultrasonic transducer is often essentially small element based arrays due to the higher frequency and the need for beam steering. An example of an ultrasound system is already given in Figure 1.6 of Chapter 1. Borrowing the terminology from radio, as the transducer in the system under discussion functions both as transmitter and receiver, the term transceiver will be used to describe the ultrasonic system used in this thesis. When the function is specific, the normal terminology will be used.

3.1.1 Piezoelectric Ultrasound Transducers

Consider an ultrasound transducer made as a plate of PZT [1] with the characteristic impedance Z_0 mounted on a backing material with characteristic impedance Z_B and connected to a load with the characteristic impedance Z_L. Surfaces of the plate are mounted with electrodes in order to drive a voltage across the plate thickness. By applying a voltage between the electrodes, the plate will be deformed due to the piezoelectric effect. The plate will either expand or contract, depending on the polarity of the applied voltage. By applying an oscillating voltage, the thickness of the plate will vibrate, and if the surface of the transducer plate is in contact with a material, the vibrations will excite an acoustic pressure wave into the material and the transducer is then acting as a transmitter. When a reflected or backscattered acoustic pressure wave hits the transducer plate surface, it excites vibrations in the surface which generates a voltage between the electrodes, and the plate functions as a receiver. Figure 3.1 gives an illustration of the plate transducer.

Resonance occurs when the transformation from electrical to acoustical energy is at it most efficient. This occurs at certain frequencies. With the PZT plate transducer, we get resonances when the plate has a certain thickness [2], given by conditions to the impedances Z_0, Z_L and Z_B. In most practical applications, $Z_L < Z_0 < Z_B$ and the first thickness resonance will occur when the plate has a thickness of half a wavelength.

$$L = \lambda/2, f_0 = c/2L \tag{3.1}$$

In situations where a large bandwidth is not needed however, such as in underwater applications, the $\lambda/4$ resonance may be used instead, as this minimizes energy loss into the backing

[1] lead zirconate titanate [15]

[2] this type of resonance is also refered to as thickness resonance

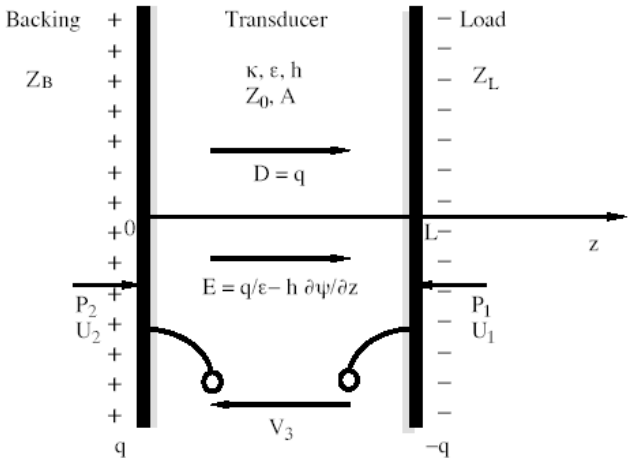

Figure 3.1: The plate transducer, cross section of piezoelectric plate, [2]

material. A $\lambda/4$ resonance can be achieved by using a very high impedance backing material [3].

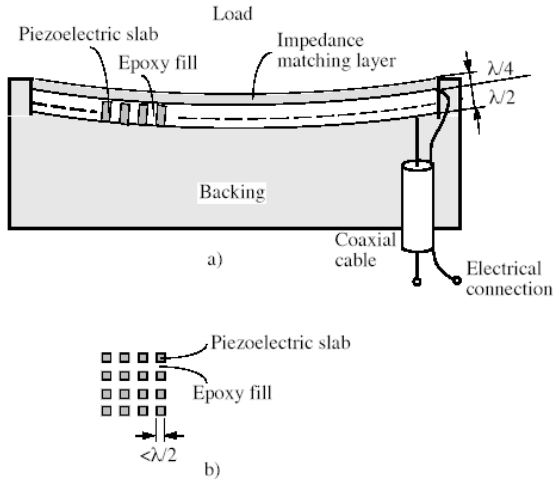

Figure 3.2: The crossection of a single element transducer made up of composite material, [2]

A typical ulatrasound tranducer is shown in Figure 3.2. The piezoelectric plate is mounted on a low impedance foam backing. An impedance transformer in form of a $\lambda/4$ thick impedance plate is attached to the front in order to increase the front vibration amplitude and to couple energy more effectively into the load. In high frequency applications (above 10 MHz), the electrodes must be taken into account of and should be treated as seperate elastic layers in addition to the impedance matching layers.

[3] ideally this means using a material with infinite impedance

To simplify analysis of the wave propagation in the transducer, it is common to assume the transducer has an infinite width and wave propagation is one dimensional and normal to the faces of the transducer. In order to avoid resonant modes outside the $\lambda/2$ wave thickness in pulse echo measurements, composite piezoelectric materials are implemented, where the the piezoelectric plate is divided into small bars of $\lambda/2$ width, and the spacing between the bars are filled with epoxy as shown in Figure 3.2. Introducing composite material also reduces reverberation artifacts and increases the energy going to the load. The one dimensional model is a simplification, though, as it does not take into account the transversal vibration modes that occur due to transversal piezoelectric coupling. These transversal modes are of larger significance in array transducers, which are composed of several elements, as opposed to the single element transducer depicted in Figure 3.2. The three dimensional shape of the piezoelectric transducer must therefore be taken account of with practical transducers. This requires three dimensional wave analysis and this can only be done numerically for certain ideal situations. Basic analysis of the transducer can however be performed using the one dimensional case, and the analysis and theory this report is based on is that of the one dimensional case. It is therefore assumed that the transducer is transversally clamped.

3.1.2 Relevant Transducer Theory

The general model that is relevant for the work done in this project is what is called the passive two port model. We say that we have a passive model of the transucer, as a passive transducer contains no internal source of power. Figure 3.3 shows the lumped electrical model of a transducer. This is found by using one dimensional analysis of the thickness vibrations on a plate transducer as shown in Figure 3.1. The pressure $p(z,t)$ and vibration velocity $u(z,t)$ are found to be functions of the plate thickness coordinate z and the time t. This analysis can also be used on focused transducers with curved plates [4].

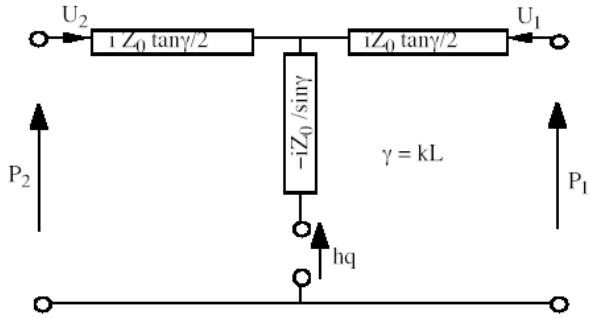

Figure 3.3: Lumped equivalent model of a transducer, [2]

3.1.3 Mason Model

In order to simplify analysis of the transducer it is common to use models. Parameters as the transmitting voltage and the transmit transfer function can be described theortically as will be mentioned in this chapter, but often it is physically hard to get these parameters directly in experiments. A thin plate of piezoelectric material with metallized electrodes as Figure 3.1 can be modelled by an equivalent circuit using standard transmission line equations. The

[4] where the radius of curvature is much larger than the plate thickness

Mason equivalent circuit of the transducer shown in Figure 3.4 is derived from the lumped model shown above in Figure 3.3, when the electrical to mechanical coupling is taken into account, in other words when h in Figure 3.3 is not zero. An ideal transformer will then convert mechanical variables into electrical variables, where particle velocities are transformed into electrical currents and pressure is transformed into electrical voltage. It is usual to focus on the energy transfer between the electric port and the front face of the transducer [5].

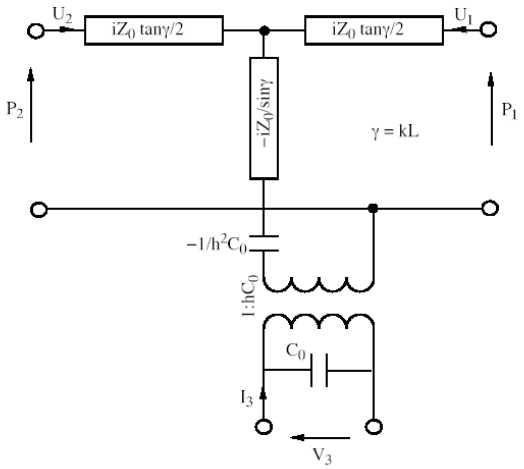

Figure 3.4: The Mason Equivalent Circuit for a piezoelectric transducer, [2]

The transmit and receive model for the transducer is based on the Mason Model, and is given below in Figure 3.5

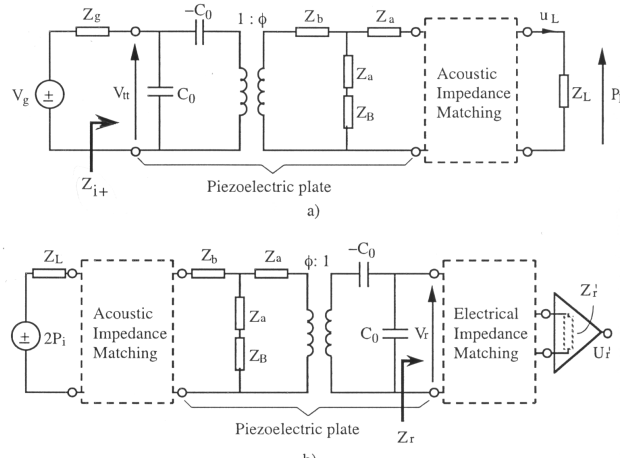

Figure 3.5: The Mason Equivalent Circuit for the transducer in transmit and recieve mode, [2]

[5] The backface is usually a load made as light as possible to improve the sensitivity, although it can in some cases be made heavy to increase bandwidth [2]

3.1.4 Transducer in Transceiver Mode

To generate a shortest possible transmit pulse, the ultrasound transducer is driven by connecting it to a fixed positive or negative voltage for a short period $T < 1/2f_0$ where f_0 is the open circuit resonance frequency [6]. A somewhat more detailed figure of the transmit and receive situation is given in Appendice III. The transfer functions in the transmit and recieve situations can be calculated using the circuits given above in Figure 3.5 as the transducer operates as a linear 2-port filter in form of a transmission line. The input impedance of the transmitting transducer is $Z_{it}(\omega)$, given as Z_{i+} in Figure 3.5. The transmitting transducer is driven by a voltage generator supplying the voltage $v_g(t)$, with an internal impedance $Z_g(\omega)$, causing a voltage drop over $Z_g(\omega)$, resulting in that the driving voltage on the electrical port of the transducer in the frequency domain is

$$V_{tt}(\omega) = H_{ti}(\omega)V_g(\omega) \tag{3.2}$$

$$H_{ti}(\omega) = \frac{Z_{it}(\omega)}{Z_{it}(\omega) + Z_g(\omega)} \tag{3.3}$$

In pulse echo applications, the drive voltage $v_{tt}(t)$ is a short burst of oscillations. This burst is then bandpass filtered by the transmit transfer function $H_{tt}(\omega)$. This is the transfer function of the combined piezoelectric plate and the $\lambda/4$ impedance matching plates of the voltage driven transmit transducer. The outcome after filtering is the velocity of the transducer, $u(t)$. In the frequency domain, the relation between the velocity and the drive voltage of the transducer is

$$U_L(\omega) = H_{tt}(\omega)V_{tt}(\omega) \tag{3.4}$$

The receiving transfer function is found by the theory of reciprocity [7].

The signal out of the receiver amplifier referred to the transducer output is given as

$$V_r(\omega) = H_{ri}(\omega)H_{rt}(\omega)2F_i(\omega) \tag{3.5}$$

$$H_{ri}(\omega) = \frac{Z_{ir}(\omega)Z_r(\omega)}{Z_{ir}(\omega) + Z_r\omega} \tag{3.6}$$

Where F_i is the force on the face of the transducer, which can also be expressed by the pressure P_i given in Figure 3.5.

The transfer function from the pressure amplitude of the incoming wave to the receiver voltage is then

$$H_{rr}(\omega) = \frac{V_r(\omega)}{2F_i} = H_{ri}(\omega)H_{rt}(\omega) \tag{3.7}$$

The transfer function from the drive voltage to the received voltage, becomes [8]

$$\frac{V_r(\omega)}{V_{tt}(\omega)} = 2H_{ri}(\omega)H_{rt}(\omega)Z_L A H_{tt}(\omega) \tag{3.8}$$

Where Z_L is the load impedance and A is the area of the transducer. In pulse echo measurements, one transducer is used for both transmit and receive as mentioned earlier in 2.2, so $H_{rt}(\omega) = H_{tt}(\omega)$. Inserting this in (3.8) gives

[6] Open circuit resonance occurs when the charge between the electrodes are constant [2]

[7] a voltage V in one branch of an electric circuit results in a measured current in another branch, shorting the voltage in the first branch and placing it in the other will result in a current I in the first branch

[8] when transmitter and receiver are in close acoustic range so power losses to beam diffraction and divergence can be neglected

$$H_{tt} = \sqrt{\frac{1}{2Z_L A}\frac{V_r(\omega)}{V_{tt}(\omega)}\frac{1}{H_{ri}(\omega)}} \tag{3.9}$$

3.1.5 Multilayered Structures and Admittance

In Figure 3.1 we see a set of piezoelectric plates with the area A, coupled to each other in layers. Usually only one of the layers is piezoelectric and is used for coupling between the acoustic and electrical energy, whilst the other layers are used for impedance matching and the forming of the frequency transfer function. A $\lambda/4$ layer between the piezoelectric plate and the load is used for impedance matching. The structure is a linear multiport structure that is given a matrix admittance [9] in the frequency domain by

$$\begin{pmatrix} \underline{I} \\ U \end{pmatrix} = \begin{pmatrix} Y & \underline{H}_{tt} \\ \underline{H}_{tt} & Y_m \end{pmatrix} \begin{pmatrix} \underline{V} \\ 2P_i \end{pmatrix} \tag{3.10}$$

Where $\underline{I}$ and $\underline{V}$ are complex amplitudes of the currents and voltages into the electric ports, U is the vibration velocity of the transducer surface, H_{tt} are the transmit transfer functions for voltage driven ports, and Y is the admittance matrix of the electrical ports when the transducer is radiating into the load. The mechanical admittance Y_m into the transducer's front face is found by setting all voltages $\underline{V} = 0$. A transducer can be fully characterized if all the components of the multiport structure matrix are known. The mechanical admittance gives an idea of the load of the transducer system, and can be found through the reflection coefficients of the transducer and the transducer's electro acoustic transfer function.

[9] the admittance is the inverse of the impedance

Chapter 4

Simulations

4.1 Transmission Line Simulations

As it is difficult to access the transducer ports directly when doing the measurements, due to inner cabling inside the transducer and the set-up as a whole, it is important to compensate for this difference. This is shown in more detail in Figure 4.1

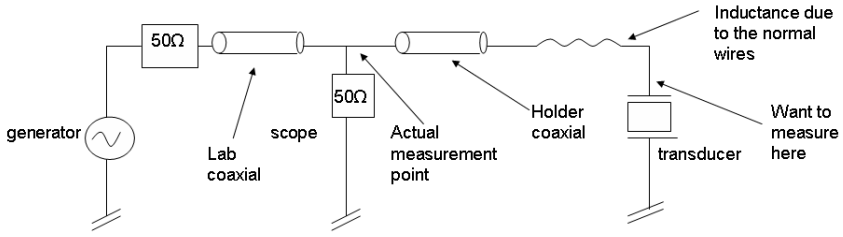

Figure 4.1: The transmission circuit

In order to find the transfer functions between the point of physical measurement and the transducer ports, the simulation program *AmpMod* was used. By allocating different ports in a given and specified circuit, the different voltage transfer functions at the different ports can be simulated and found. Below in Figure 4.2 and in Figure 4.3, the different ports at transmission and reception are shown respectively.

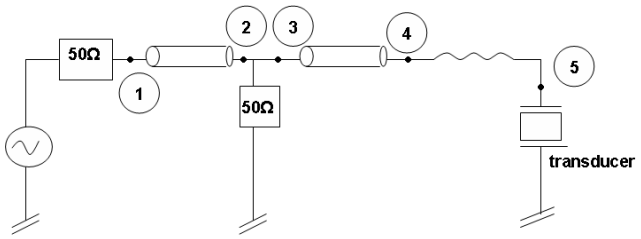

Figure 4.2: Model for transmission mode simulation

It can be observed that the ports in transmission mode and reception mode are numbered differently, as port 1 in transmission mode is by the pulse generator, whilst port 1 in reception

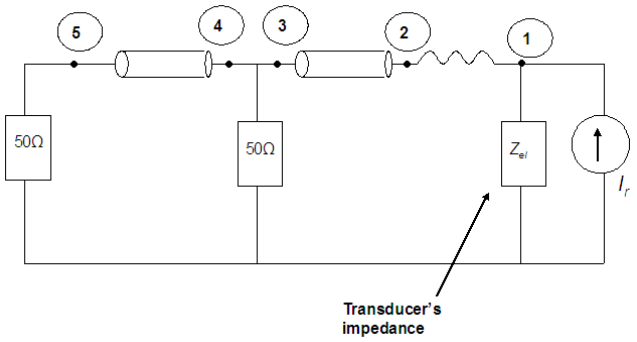

Figure 4.3: Model for reception mode simulation

mode in by the transducer.

The program *AmpMod* compensates for all the unwanted elements caused by the fact that we are measuring at port 3, and not in the port of interest 5 in the transmission mode situation, shown in Figure 4.2, corrosponding to port 3 and port 1 in the receive situation, seen in Figure 4.3. However the input impedance is different in transmission mode and reception mode, where in transmission mode the input impedance is dependent on port 2 in in Figure 4.2, while in reception mode, the input impedance is dependent on port 5 in Figure 4.3. However, we assume a negligeble difference between the input ports in the transmission and reception situation, since both are connected to the same coaxial cable and a 50Ω impedance. In transmission mode, 50Ω will be seen from port 2 in Figure 4.2, and in reception mode, 25Ω (two 50 Ω in parallell) will be seen from port 5 in Figure 4.3, which is not much of a difference.

The expression for the transfer function is dependent on the voltage in transmission mode given in the previous chapter, in Equation (3.9). This is the voltage at the transducer ports, which is physically impossible to access, and hence compensation is needed to transform the actual measured voltage into the desired voltage at the transducer ports.

Let V_{t5} be the desired voltage at transmission mode and V_{t3} be the physically accessible and measured voltage at transmission mode seen in Figure 4.2. Similarly, V_{r1} is the desired voltage at reception, and V_{r5} is the physically accessible and measured voltage at reception mode seen in Figure 4.3, where the numbers in the subscript for the voltages all represent the port numbers in the respective figures in the transmit and the receive situations.

The following relations in Equations (4.1),(4.2) and (4.3) are then given, where the voltage transfer functions at each port is included.

$$V_{t5} = V_{t3} \cdot \frac{H_t 5}{H_{t3}} \tag{4.1}$$

In reception mode, the following equation is valid

$$V_{r1} = V_{r5} \cdot \frac{H_{r1}}{H_{r5}} \tag{4.2}$$

Combining the two equations above, an expression for the transfer function between the voltages between the desired and the actual voltages at transmission and reception are obtained

$$\frac{V_{r1}}{V_{t5}} = \frac{V_{r5}}{V_{t3}} \cdot \frac{H_{r1}}{H_{r5}} \cdot H_{t3} H_{t5} \tag{4.3}$$

Where the expression

$$H = \frac{H_{r1}}{H_{r5}} \cdot \frac{H_{t3}}{H_{t5}} \tag{4.4}$$

is the transfer function between the desired and actual voltages measured in the given set-up, giving the expression

$$V_{r3} = V_{t5} \cdot H \tag{4.5}$$

For the reflection coefficient however, these compensations are not nescessary, as the transfer function between the voltage at the desired measuring port and the actual measured voltage gets eliminated in the expression for the reflection coefficient as seen below in (4.7). The reflection coefficient is found by

$$R_T = k(f) \cdot \frac{V_{tx,e2}}{V_{tx,e1}} \tag{4.6}$$

Where $V_{tx,e1}$ and $V_{tx,e2}$, are the voltages measured at port 5 at transmit corrosponding to Figure 4.2, of echo number one and two in the frequency domain, and $k(f)$ is a frequency dependent function that includes the attenuation in water and the reflection coefficient between water and brass explained more in detail in Chapter 5.

Using the experimentally measured voltages, measured at port 3 at transmission, corrosponding again to Figure 4.2 the reflection coefficient is found to be the same as in (4.6)

$$R_T = k(f) \cdot \frac{V_{tx,e2} \cdot H}{V_{tx,e1} \cdot H} = k(f) \cdot \frac{V_{tx,e2}}{V_{tx,e1}} \tag{4.7}$$

And hence we see that the reflection coefficient is independent of where in the circuit the measurements are taken with respect to port 3 and port 5 in transmission mode.

4.2 Parameters inserted in *AmpMod*

The components in Figure 4.2 and Figure 4.3 where all inserted as blocks in the MATLAB subroutine *AmpMod*. The impedance values for the pulse generator, the coaxial cables and the oscilloscope were all taken from datasheets and specifications. Impedance measurements were taken however, as the non coaxial cables were expected to contribute with a parasetic inductance as shown in Figure 4.1. This inductance includes contributions from both the visible non coaxial cables outside the transducer and the hidden non coaxial cables inside the transducer. The value of the complex inductance with inductance compensation Z_{comp}, was found by measuring the complex impedance impedance of element 1 at the array holder Z_{array} where the non coaxial cables were soldered onto the coaxial cables as shown in Figure 4.4, and then subtracting this with the impedance due to the inductance L, where the impedance of L is given as $Z_L = j\omega L$, shown below in Equation (4.8). The value of the inductance L was obtained by trying to get the phase information as near $-90°$ as possible at 40 MHz, without overly distorting the impedances and phases. By taking these points into consideration, the parasitic inductance L was estimated to be around L =70 nH. Figure 4.5 shows the impedance without inductance compensation, and with inductance compensation.

$$Z_{comp} = Z_{holder} - Z_L = Z - j\omega L' \tag{4.8}$$

The other components were as mentioned found using the datasheets of the coaxial cables and the oscilloscope and generator. The capacitance for the coaxial cables were given as 94 pF/m thus giving the inductive value of

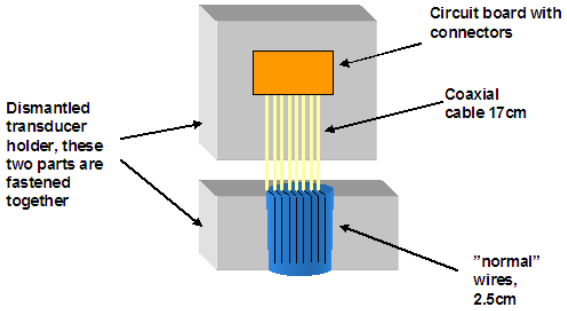

Figure 4.4: The different wires and cables between transducer and connectors

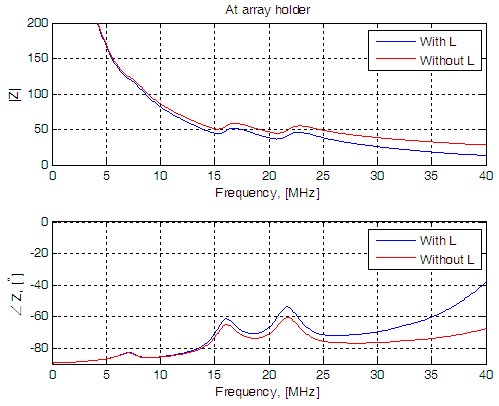

Figure 4.5: Impedance with and without inductance compensation

$$L = Z^2 \cdot c = 50^2 \cdot 94 \cdot 10^{-12} = 235nH/m \tag{4.9}$$

The impedance due to the resistance of the coaxial cables was chosen to be a small number, where 0.1 was chosen for practical purposes. The component blocks inserted in the *AmpMod* program both under transmission and reception, are given more in detail in Table 4.1.

Table 4.1: Component values in *AmpMod*

Component/Block	Impedance [Ω]	Capacitance [pF]	Inductance [nH]	Length [m]
Input impedance, pulse generator	50	-	-	-
Coaxial cable	0.1	94	235	2
Oscilloscope	50	-	-	-
Coaxial cable	0.1	94	235	0.17
Inductance	-	-	70	-

4.3 Implementation of the Simulation to the Measurement Results

After inserting a circuit with parameters corresponding to the one used in the measurement set-up, the different voltage transfer functions involved in the main voltage transfer function H given in Equation (4.4) were taken from a file scm_zup_res given by the *Ampmod* simulation program, and interpolated in order to be used with the measurement data, using the *interp*1 function in MATLAB. After doing that, it was only a question of multiplying the measured data with the voltage transfer function H in order to get the desired value V_{t5} and V_{r1} as shown in Figure 4.2 and Figure 4.3. Below the transfer functions for the voltages at the different ports in transmit mode and receive mode corresponding to the circuits given in Figure 4.2 and Figure 4.3 respectively are given in Figure 4.6. When considering voltages, port 2 and 3 are equivalent in both transmission and reception mode.

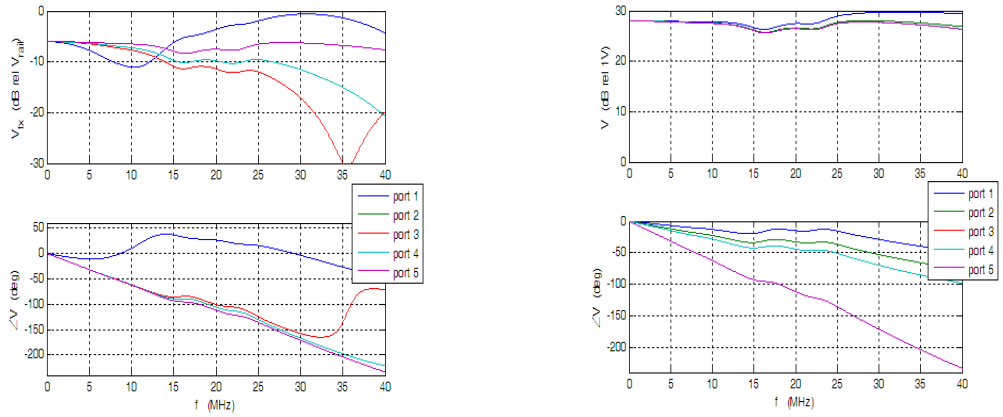

(a) Voltage transfer function during transmission (b) Voltage transfer function during reception

Figure 4.6: Voltage transfer functions

It can be observed from Figure 4.6 that there is a considerable difference between the voltage transfer function at port 3 and the voltage transfer function at port 5.

4.4 Parameter Simulations

The electro acoustical transfer function at transmission, explained in the previous chapter in Equation (3.9) and the reflection coefficients of a 20MHz transducer with 1 layer was also simulated, in order to get an idea of what was to be expected of the results. This was done using a simulation program in MATLAB called *xtrans*. The parameters used to model the transducer are given in the appendix. Below in Figure 4.7, the simulated electroacoustic transfer function, H_{tt} and the reflection coefficient, R_T for the transducer are shown [1].

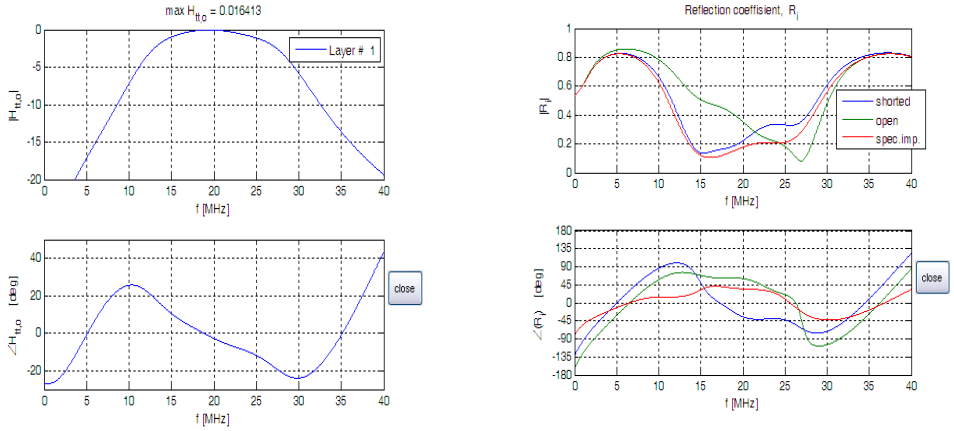

(a) Simulated H_{tt}

(b) Simulated R_T, red plot

Figure 4.7: The simulated values of H_{tt} and R_T

The phase given for H_{tt} generated by the simulation program *xtrans* in MATLAB shown in Figure 4.7 is however programmed in such a way that a straight line is subtracted from the phase value in order to remove effects of time delays. Figure 4.8 therefore shows a more realistic plot of the phase for H_{tt}, obtained directly from the simulated value of the parameter H_{tt}.

By approximating linearity and finding the slope of the plot in Figure 4.8, an idea of the time delay $\tau_{simulated,H_{tt}}$ of the system can also be found, given by the following expression

$$\tau_{simulated,H_{tt}} = \frac{\Delta\angle H_{tt}}{\Delta\omega} \tag{4.10}$$

and is found to be 47.7 ns by using the above equation and inserting $\Delta\omega = 2 \cdot \pi \cdot \Delta f$ and converting the degrees to radians in $\Delta\angle H_{tt}$. This corresponds to approximately 1 period of a 20 MHz transducer. It is assumed that the pulse propagates approximately one period into the transducer, from the electrodes to the transducer plates.

[1] note that the red plot is the relevant plot

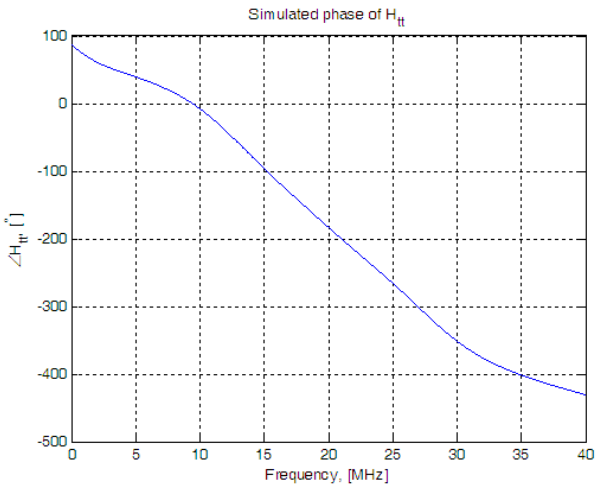

Figure 4.8: The phase of the transfer function H_{tt}

Chapter 5

Instrumentation and Measurement Set-up

Details in the measurement setup and instrumentation is given in this chapter. The equipment used is specified. The measurements were performed in bubble free water, as bubbles scatter the signal, a highly undesirable effect for the measurements taken in this project.

5.1 General instrumentation and measurement set-up

5.1.1 Pulse echo measurement set-up

The transducer holder was mounted on the robot and coaxial cables were coupled directly from the transducer holder to a digital oscilloscope and an arbitrary waveform generator. The electronics of the holder is explained below. It was intended that the signals go straight from the Arbitrary Waveform Generator to the transducer, and back, where the generator acts as a pulser and a receiver. This was done by putting the coupling of the oscilloscope to 1MΩ. However, this resulted in some unexpected behaviour, resulting in that the coupling on the oscilloscope was set to 50Ω. Reasons for this is given in Chapter 6. Different types of pulses were programmed from and into the arbitrary waveform generator and sent into the transducer, using a software called ArbConnection. The pulses and the echoes shown in the digital oscilloscope were recorded using a regular laboratory PC using a MATLAB program *laap* (Lab Application), also used to control the oscilloscope with respect to setting delays, when manually turning of knobs was tedious and inaccurate. An overview of the measurement setups are shown more in detail in Figure 5.1, Figure 5.2 and the practical setup in the laboratory is shown in Figure 5.3.

Coaxial Cable used between Connectors, Oscilloscope and Generator

The coaxial cables that were plugged directly to the oscilloscope and the Arbitrary Waveform generator, were 2m long 50Ω with BNC plugs on one side and MCX plugs on the other, in order to connect to the connectors on the circuit board.

The Pulses used in the Measurements

There were two kinds of pulses used in the experiments, and these were sinusoidal burst pulses and Gaussian pulses, with different frequencies. The sinusoidal burst is a often used to characterize transducers in NDT applications. In addition to this, it has a broad bandwidth. The

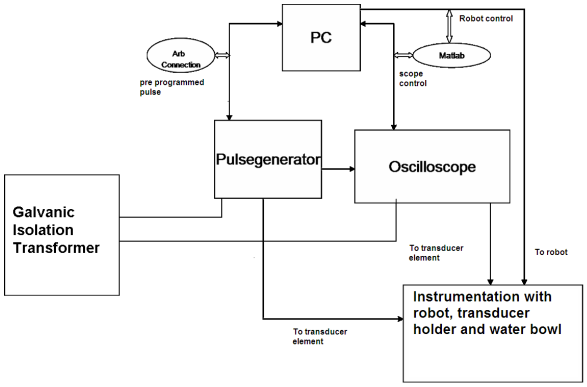

Figure 5.1: Hardware and software used in the measurement set-up

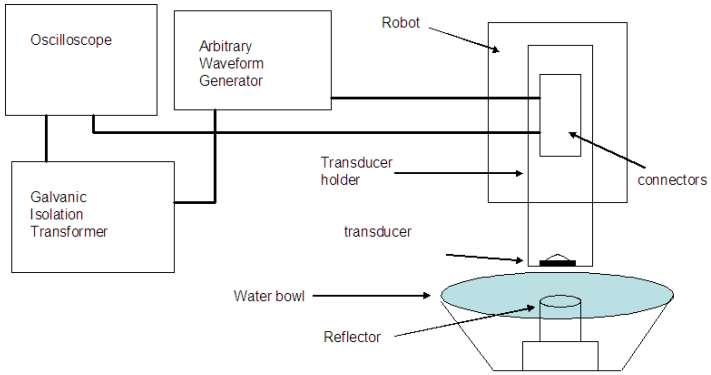

Figure 5.2: Measurement overview of the set-up

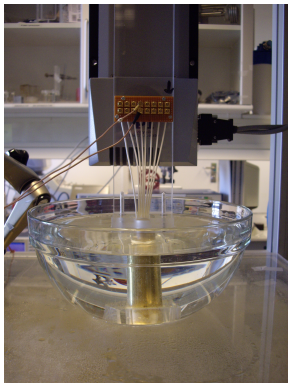

Figure 5.3: Practical set-up in lab

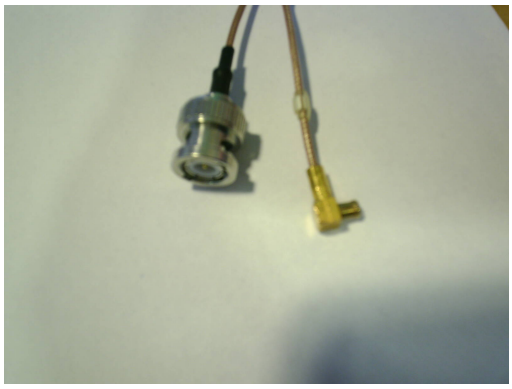

Figure 5.4: Connectors used in the measurement set-up, MCX for the circuit board and BNC connected to the oscilloscope or generator

Gaussian pulse has more limited bandwidth, and can in this way have desirable characteristics. Another important observation is that the smaller a Gaussian pulse, the more it resembles a δ function, and hence the temporal response will become more like the inverse Fourier transform of the system transfer function [1]. The Gaussian pulse also has lower sidelobes than the sinusoidal pulse. Figure 5.5 and Figure 5.6 give examples of the pulses and their frequency spectra. The frequency range of interest, is approximately 0-40MHz, and the pulses used in this example were taken via the oscilloscope when coupled to the waveform generator.

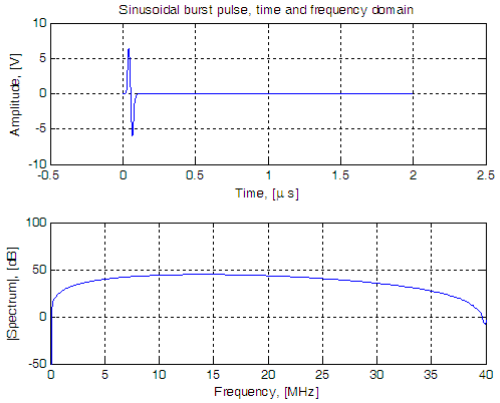

Figure 5.5: Sinusoidal burst pulse

It can be observed that the sinusoidal burst pulse has a very broadbanded frequency spectrum, it has nearly a 70 percent bandwidth, and this can be interesting to use as there is some energy in all the frequencies in the area of interest, mainly from 10 to 40 MHz.

As seen in Figure 5.6, the Gaussian burst pulse has slightly more limited bandwidth than the sinusoidal pulse. The complete spectral information shows that the Gaussian pulse had lower sidelobes for $f > 40$MHz than the sinusoidal pulse. However, in the range of interest, we see that the Gaussian had slight sidelobes compared to the sinusoidal, which did not have any.

[1] by taking the inverse Fourier transform of a system fed with a δ function, the direct system response can be found

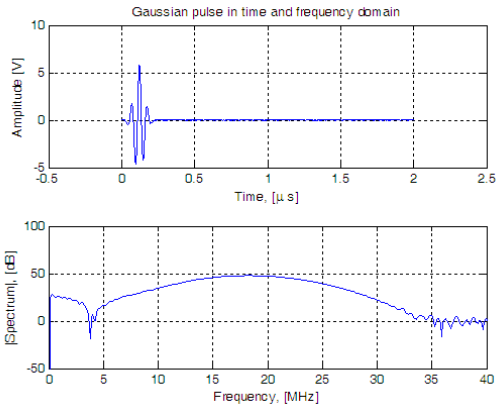

Figure 5.6: Gaussian burst pulse

The sinusoidal burst pulse was programmed directly from ArbConnection and it was given an amplitude of 16V.

The Gaussian pulse was first made in MATLAB using the function *gauspuls*, creating a Gaussian modulated sinusoid. This was a 50 kHz Gaussian RF puls med 60 percent bandwidth og truncate pulse where it falls 40 dB below the peak and a samplerate of 1MHz. It is then converted into a 16 bit representation, and then using the built in MATLAB functions *fid*, *fopen* and *fwrite* to create and store the pulse in $*$.wav format. After that it was downloaded into the Waveform Generator using the ArbConnection software. The Gaussian pulse was constructed in such a way that its spectrum had a peak at around 20 MHz. Generally when creating a self defined pulse in ArbConnection, as was done with the Gaussian pulse, the desired frequencies are picked by a variation of the pulse length or the sampling frequency to create a signal with a desired frequency spectrum. This frequency was therefore selected by altering the number of points in the MATLAB code used to generate the pulse. The sampling frequency used was 242 MS/s, and in order to have a peak around 20 MHz, the four period Gaussian pulse created in Matlab was to have approximately 48 points. The relationship between these values are given in Equation (5.1) and Equation (5.2) below

$$T_{gaussian}[s] = \frac{N_{pulse}}{4} \cdot T_{sample,generator} = \frac{N_{pulse}}{4} \cdot \frac{1}{f_{sample,generator}} \tag{5.1}$$

Rearranging the above equation to obtain the frequency of the Gaussian pulse gives

$$\frac{1}{T_{gaussian}} = f_{gaussian} = \frac{242MS/s}{48S} \cdot 4 \approx 20[MHz] \tag{5.2}$$

5.1.2 Instruments used for the Measurements

Below is a list of the equipment in the laboratory used for the measurements

Optimal Positioning with Robot

After positioning the transducer in the best way possible into the geometrical focus of the reflector by looking at the amplitude and duration of the echoes, a 3d-scan was performed in order to obtain the optimal positioning of the transducer with respect to the reflector. The software used to perform the 3d-scan was *laap*. The 3d-scan was performed by first doing a

Table 5.1: Main laboratory equipment used in the measurements

Instrument	*Type*	*Registration nr*
Pulse Generator	Tabor Electronics Waveform Generator (250 MS/s)	00810
Oscilloscope	Lecroy Waverunner LT262 350MHz 1GS/s	00391
HP4194 Impedance Analyzer	-	-
Galvanic power transformer	-	-

scan in the z direction (the axial direction), where the optimal distance between the transducer and the reflector was obtained. After that, scans in the x and y directions were performed to find the best lateral positioning. The data was then processed and the best pulses from the optimal position was chosen for further data processing by looking at the radiation profile from the scans. The radiation profiles were acquired directly by using the inv_{2dscan} function in the lab application (*laap*) software. An example of such a radiation profile is shown in Figure 5.7 and Figure 5.8, and it was observed that all the echoes had their maxima at the same position, as opposed to what was observed in the work done previously, [19]. This indicates that the constructed reflector served its purpose, as it didn't corrode in water causing unexpected results. In order to verify that the echoes all had maximal values at the same scan position, a 3d scan was performed on all the echoes, in all the depths. The depths were varied by varying the time delay between the transmitted and the reflected pulse. The time delay between the echoes were selected to be in the range from 2.2 μs to 4.3 μs, corresponding to a distance of 1.65 mm to 3.23 mm with an increment of 0.2 mm between the transducer and the reflector.

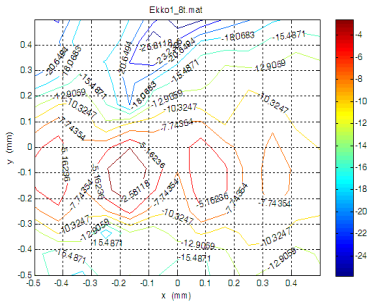

(a) Contour diagram for echo 1

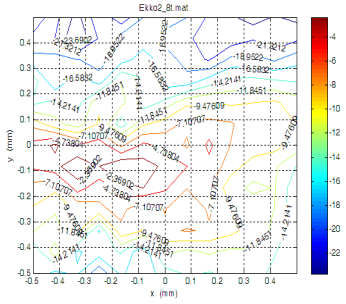

(b) Contour diagram for echo 1

Figure 5.7: Contour diagrams matching in optimal position

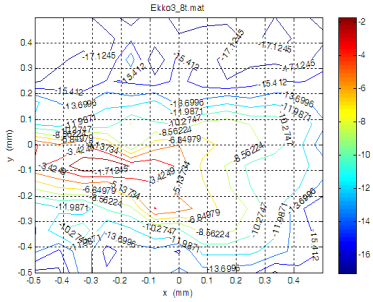

(c) Contour diagram for echo 3

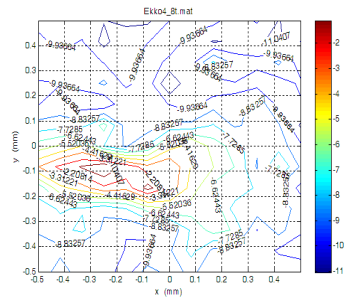

(d) Contour diagram for echo 4

Figure 5.8: Contour diagrams matching in optimal position

The optimal axial distance between the transducer and the reflector is expected to be somewhere close to the following calculated value. As the geometrical focus of the transducer is at $z_T = 27,5$mm, and the radius of curvature for the reflector is $z_R = 25$mm, the transducer should be around $\Delta z = z_T - z_R = 2,1$ mm away from the reflector surface. As it is not possible with the given equipment to accurately measure the distance in length from the transducer to the reflector, time considerations between the first and the second echo are observed in order to then be able to calculate the distance between the transducer and the reflector. For this, it is a simple question of linear displacement as the time between two consecutive echoes is given as

$$t = 2d/c \tag{5.3}$$

Where t is the time between two consecutive echoes, d is the distance between the transducer and the reflector, and c is the speed of sound in water, given as 1492 m/s [4]. The desired time between two echoes is then found using equation (5.3), to be 2.8μs. This is seen manually on the oscilloscope, by observing the time between the first and the second echo. By recording pulses and echoes around the desired distance of 2.12 mm, the optimal distance is found.

5.1.3 Impedance Measurements

The impedance measurements were taken with an HP impedance analyzer, after compensating for the impedance due to the connecting wires from the transducer to the impedance analyzer. Open and short circuit compensations were performed on the wires, and then the impedances were measured at each element at the connectors on the circuit board on the transducer holder. The impedance analyzer was coupled to the laboratory PC, and the data was recorded by using a software on the PC called *impMeasure*. In order to see the effects of the coaxial wires soldered onto the normal wires on the signals, an impedance measurement at the termination of the normal wires was also done in order to see the coaxial cabling effects. This is presented later in the Chapter 7.

5.2 The Transducer Holder

The transducer holder was designed in order to ensure that the transducer is held fixed and parallell to the water surface. It is initially a small block with a hole slightly larger than the diameter of the transducer, where the transducer fits in, and then sealed using epoxy. By fitting the transducer into this pipelike hole only slightly larger than itself, it is secured against tilting and remains fixed in position. The holder and the transducer is therefore a component in the measuring system displayed in Figure 5.2. Below in Figure 5.9 the designed transducer holder in different angles is presented.

5.2.1 The Electronics in the Transducer Holder

The normal wires connected to the element pads of the transducer were cut and 50Ω coaxial wires were soldered onto these. As it was desired to have two connectors for one element, two coaxial wires were soldered onto the normal wire coming from each element on the transducer pad. The coaxials where then soldered onto MCX connectors on a regular circuit board. As the transducer had 8 elements, and each element had two connectors; one for coupling to the oscilloscope,and one for coupling to the pulse generator, the circuit board had altogether 16 connectors on it. In order to connect the elements to the oscilloscope and waveform generator, a new pair of 50Ω coaxial cables where used, with BNC plugs on one side, to couple to the

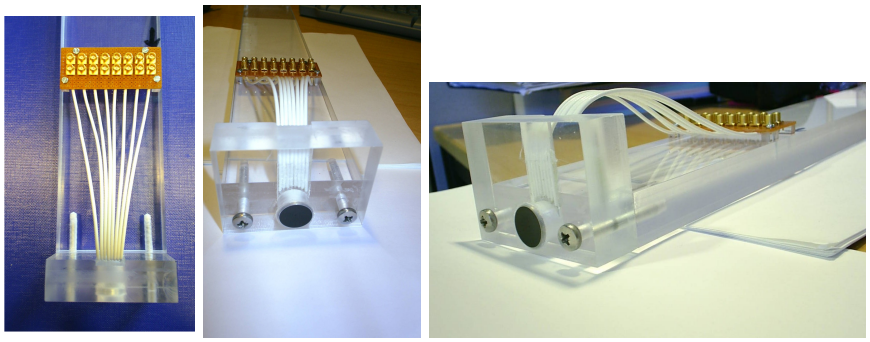

Figure 5.9: The transducer holder in different perspectives

oscilloscope and the waveform generator, and MCX plugs on the other side, to plug into the connectors on the circuit board leading to the elements.

Coaxial Cable used between the Normal Wires and the Connectors

The coaxial cables used were 50Ω RGB cables,and they were approximately 17 cm in length. With the capacitive value and calculated inductive values of 235 nH/m given in Equation (4.9), and with the coaxial wires being 17 cm, the capacitive and inductive value this wire introduces into the system, is $94 \cdot 0.17 = 16$pF and $235 \cdot 0.17 = 40$nH respectively.

Normal Wires

The normal wires were the wires directly soldered onto the transducer pad, and these were approximately 2.5 cm long. Figure 4.4 in the previous chapter shows how the transition between the normal wires from the transducer pad and the coaxial wires are, when looking at the dismantled transducer holder, where one part is the plate with the circuit board on it, and the other part is the plate with the transducer itself. The lengths of the cables are also given.

5.2.2 The Transducer

The transducer used in this work was a Panametrics 3853B102 annular array focused transducer, with a center frequency of 20 MHz, the 5 first elements having a radius of curvature of 27.12 mm. Annular array transducers hold certain advantages to high frequency single element transducers, as single element transducers have limited focal depth and deterioration of the image quality beyond the focal zone of the one element. By using arrays, dynamic reception focusing can be achieved by introducing time delays to each element of the array, thus improving the depth of focus and retaining the same resolution as a comparable single element transducer. The annular array maintains nearly uniform lateral resolution thus getting a better depth of field [5]. An annular array transducer consists of several concentric rings, and a steerable focus is obtained by putting a spherical delay on the excitation signals for the different elements. The transducer used here is constructed in such a way that element 1 has a small hole in it for design purposes, in order to align the elements to one another. This will influence the impedance of the element, as the effective area is reduced, and as the impedance is inversely proportional to the area of the element. Other characteristics as the reflection coefficients and transfer function can also vary due to this. Element 1-5 have the same area, with the ring diameter being 1.9 mm. Element 6 is twice the area of element 1, element 7 is thrice the area and element 8 is four times the area of element 1.

5.3 The Reflector

The reflector was chosen to be a cylindrical brass reflector with a curved top, with the same radius of curvature as the focused transducer. It was slightly slanted at the bottom, to avoid unwanted echoes from the bottom dispering with the echoes from the top of the reflector. The reflector used is shown below in Figure 5.10.

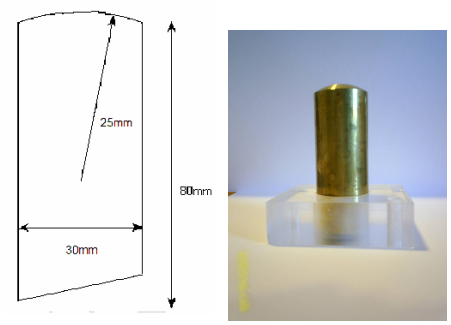

Figure 5.10: Geometrical specification sketch and actual reflector with holder

5.4 Preliminary Results and Calculations

5.4.1 The complex electroacoustic transfer function

The electro acoustic transfer function is found by using the expression in Equation (3.9). However, there are some important considerations that should be accounted for, as both V_{tt} and the time delay compensation should be compensated for, as $V_{tt,measured}$ should be multiplied by the transfer function found in the third chapter, given in Equation (4.5), in order to find the desired voltage at the transducer ports in transmit mode, V_{tt}, given in the theoretical Equation (3.9). Since the complex transfer function is desired, it is also important to get the right phase information, and in order to do that, time delay compensation in water should be done, as the pulses also travel the distance between the transducer and reflector in the water. This is described in the following section.

Time Delay Compensation in Water

As the transfer function is complex, the time delay should be accounted for. There are two main time delays that should be accounted for in the set-up, the first one being the time delay due to the pulses' travel path in the water, called τ between the transducer and the reflector, and the second being the time delay the pulses go through the electrical circuit leading to the transducer ports, called τ_2. The simulation model explained in Chapter 4 deals with the delay τ_2.

The time delay between the transmitted pulse $V_{tt,measured}$ and the first echo is not the best way to obtain the time between two echoes, as the wires inside the transducer also contribute to the delay. Therefore, the time between the first and the second echo is obtained by finding the value where the respective pulses start. This can be done, by measuring the beginning of these pulses. Internal reflections inside the transducer itself do not affect the measurements, as illustrated in Figure 5.11. This contributes to an added time delay, and an added uncertainty due to a lack of knowledge as to where the acoustic pulse starts between the ports of the transducer.

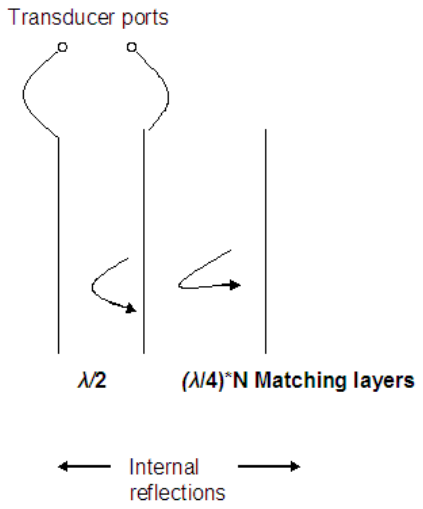

Figure 5.11: Internal reflecions inside the transducer

By measuring the time at the beginning of the pulses, and then taking the time difference between two consecutive pulses, the best ones being echo 1 and echo 2, as the pulses get stretched in time the higher the echo number is[2], one can therefore establish the time delay in the water-path using the time difference between two consecutive echoes.

However, as the expression for the transfer function is dependent on pulses and echoes in the frequency domain, it is important to be aware that the time windows for the different echoes are not the same, so the *fft* in MATLAB will start where the time window starts. The time window must therefore also be compensated for in the expression of the time delay due to the propagation in water. The time delay in water is

$$\tau_{water} = t_{echo,2} - t_{echo,1} \tag{5.4}$$

Where t_{echo2} is the time measured at the start of echo number two, and t_{echo1} is the time measured at the start of echo number one. With a reference point at $t = 0$, the following relationship between the measured pulse and desired pulse in the Fourier domain exists

$$V_{tt}(f) = V_{tt,m}(f) \cdot e^{-j\omega t_{0,V_{tt}}} \tag{5.5}$$

Where $V_{tt,m}(f)$ is the measured echo and $V_{tt}(f)$ is the voltage without the time delay caused by the oscilloscope window. This time delay is given by the factor $e^{j\omega t_{0,V_{tt}}}$ specified by the window of the oscilloscope.

Similarly, the expression for echo 1 is given as

$$V_{tx,e1}(f) = V_{tx,e1,m}(f) \cdot e^{-j\omega t_{0,e1}} \tag{5.6}$$

In addition to this, there is also the time delay caused by the pulses' travelpath in the water, as mentioned in Equation (5.4). As this delay contributes with a factor of $e^{-j\omega\tau_{water}}$, this is compensated for by multiplying with the factor $e^{j\omega\tau_{water}}$, as this eliminates out the delay. This gives the following expression

[2]when doing the pulse echo measurements, stretching in time was observed, especially in the third and the fourth echoes

$$\frac{V_{tx,e1}(f)}{V_{tt}(f)} = e^{-j\omega\tau_{water}} \frac{V_{tx,e1,m}(f) \cdot e^{-j\omega t_{0,e1}}}{V_{tt,m}(f)} \tag{5.7}$$

Table 5.2 below gives the different values for the time delay in water and the recorded delays from the oscilloscope window for the different pulses.

Table 5.2: Time delay in water and the recorded delays from the oscilloscope

Pulse type	Element number	$\tau_{water} = t_{echo,2} - t_{echo,1}$,[$\mu$s]	$t_{0,V_{tt}}$[ns]
Gaussian	1	2.7597	-0.5000
Sinus Burst	1	3.1379	-0.5000
Gaussian	2	2.7070	-0.5000
Sinus Burst	2	2.9435	-0.5000

The time delay introduced into the electrical circuit due to the difference in the actual measurement point and the optimal measurement point can be found by the relationship between the measured signal, and the desired signal of interest, as indicated in Chapter 4 in Equation (4.3) and Equation (4.4).

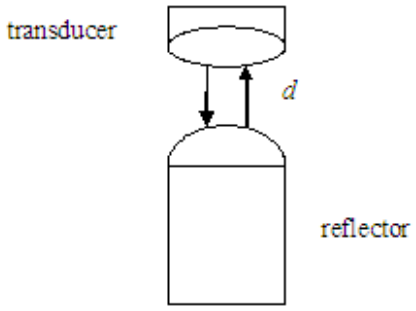

Figure 5.12: The transmitted and reflected pulses from transducer to reflector

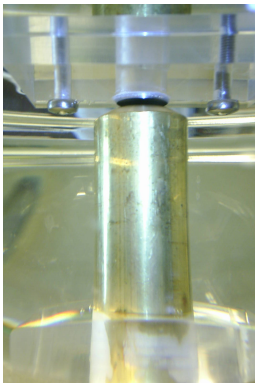

Figure 5.13: Transducer/reflector arrangement in water

Reflection Coefficients

In order to obtain the modulus and phase of the reflection coefficients from the data obtained, the following formula was used, as the coefficients are the relationship between two consecutive echoes in the frequency domain. Physically, the pressure wave P_0, with a corrosponding voltage amplitude V_0 travels from the transducer and gets reflected at the reflector surface. However, the reflection coefficient between water and brass, and the attenuation in the waterpath the pulse travels should also be taken into consideration, as shown in Figure 5.14, giving the following expression for the reflection coefficient for the transducer,

$$R_{T,n+1,n} = \frac{V_{n+1}}{V_n} \cdot \frac{1}{R_{wb} \cdot \alpha^2} \tag{5.8}$$

where n is the echo number, explaining whether it is the first, second, third or fourth echo, R_{wb} is the reflection coefficient between water and brass and α is the attenuation in water. The reflection coefficient between water and brass is given by the following expression

$$R_{wb} = \frac{Z_b - Z_w}{Z_w + Z_b} = \frac{\rho_b c_b - \rho_w c_w}{\rho_w c_w + \rho_b c_b} \tag{5.9}$$

where Z_w is the acoustic impedance of water and Z_b is the acoustic impedance of brass, given as $37.30 \cdot 10^6$ kg/m^{2}s, [20][3]. The acoustic properties of air free water at 1atm at 20°, is given as $\rho_w = 998.2071$kg/m^3 [11]. The acoustic impedance of water, is then given as $Z_w = \rho_w \cdot c_w = 1.4893 \cdot 10^6$kg/m^{2}s, when using a speed of sound in water given as $c_w = 1492$ m/s. By inserting the values given for Z_w and Z_b, the value for the reflection coefficient between water and brass becomes $R_{wb} = 0.9232$. The logarithmic attenuation in water, $\alpha_{dB,cm}$ is given by the frequency dependent attenuation expression [1]

$$\alpha_{dB,cm} = 2.17 \cdot 10^{-15} \cdot f^2 [dB/cm] \tag{5.10}$$

So, in order to use the attenuation formula directly in the expression for the reflection coefficient, $\alpha_{dB,cm}$ should be multiplied by the distance the pulse travels in cm, and converted into a non logarithmic scale, as given below

$$\alpha = 10^{0.1 \cdot 2.17 \cdot 10^{-15} \cdot f^2 [dB/cm] \cdot \Delta d} = 10^{0.1 \cdot \alpha_{dB,cm} \cdot \Delta d} \tag{5.11}$$

where Δd is the distance the pulses travel in water, also the distance between the transducer and the reflector. With all the above values inserted, the expression for the reflection coefficient finally becomes

$$R_{T,n+1,n} = \frac{V_{n+1}}{V_n} \cdot \frac{1}{0.9232 \cdot 10^{0.434 \cdot 10^{-15} \cdot f^2 \cdot \Delta d}} \tag{5.12}$$

The phase of the reflection coefficients was established by adding the time delay compensation in water to the complex expression of the reflection coefficients, as done with the electro acoustic transfer function above. The phase characteristics can be obtained using two consecutive echoes reflected between the reflectors surface and the transducer. The phase shift between two consecutive echoes can then be found due to the pulses' travelling path in water. This is done directly in the Fourier domain by multiplying the expression for the reflection coefficient by the factor $e^{j\omega(\tau_{water} + e_{n,t_0} - e_{n+1,t_0})}$, similar to the factor given in Equation (5.7), and then using the *unwrap*[4] and *angle* function in MATLAB to directly obtain the phase of the reflection coefficients. Part of the expression used to obtain the phase of the reflection coefficients is given below

[3] This was the numerical value of the acoustic impedance of naval brass

[4] to prevent the phase jumping +180 degrees for each crossing of the negative real axis

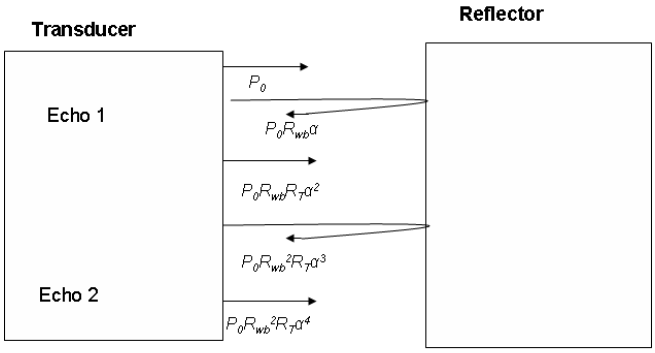

Figure 5.14: Ultrasonic propagation path between the transducer and reflector

$$\frac{V_{n+1}}{V_n} = \frac{V_{n+1,m}e^{-j\omega(V_{n+1,t_0})}}{V_{n,m}e^{-j\omega(V_{n,t_0})}} \cdot e^{j\omega\tau_{water}} \tag{5.13}$$

Where τ_{water} is found as the difference between the first and the second echo.

Chapter 6

Results

In this chapter, the main results are be presented, these being the reflection coefficients, and the electro acoustic transfer functions. All measurements were done mainly on element 1 and element 2 of the transducer array.

6.1 Electroacoustic Transfer function

When calculating the transfer function in MATLAB using Equation (3.9), a variation of the square root was used in MATLAB, as taking the square root directly created troubles due to that the *fft* operation recognized two numbers, and therefore centered most of the signals in the right side of the polar plot. The *sqrt()* function in MATLAB was therefore interchanged with the following relation

$$\sqrt{x} = \sqrt{|x|} \cdot e^{j\angle x/2} \tag{6.1}$$

The electro acoustical transfer functions and their phases obtained for Gaussian and sinusoidal burst excitations for element 1 are given in Figure 6.1. The signals used to calculate the transfer function are unfiltered, but the DC components have been removed from echo 1 of both the signals.

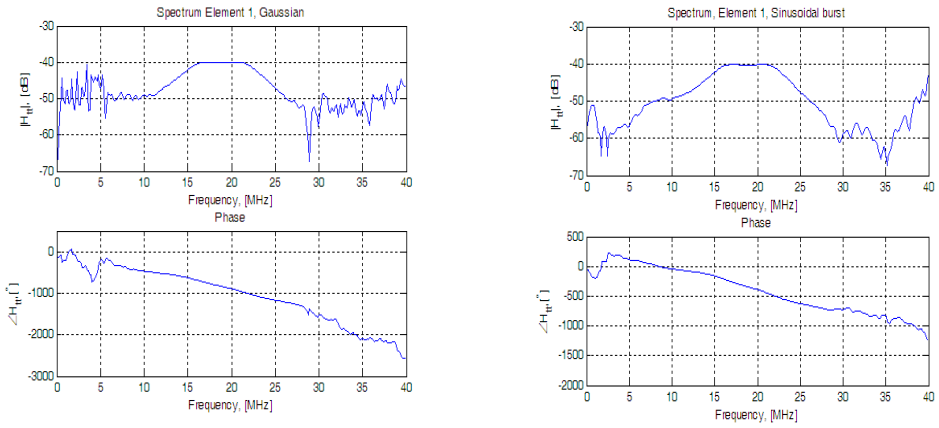

(a) H_{tt}, Gaussian (b) H_{tt}, sinusoidal

Figure 6.1: Complex electroacoustic transfer functions for element 1

It can be observed that the amplitude characteristics are flat for both the sinusoidal and gaussian pulse in the region 15-22 MHz. Possibly this is because the transducer has been custom designed for operation in and around 20 MHz. The amplitude characteristics will therefore be flat having its peak value in the set region.

Corrosponding results are given for element 2, where Figure 6.2 show the complex electro acoustical transfer functions of element 2, for a Gaussian and a sinusoidal excitation. As in the case of element 1, the DC component of the echo signal has been removed but otherwise no filtering was done.

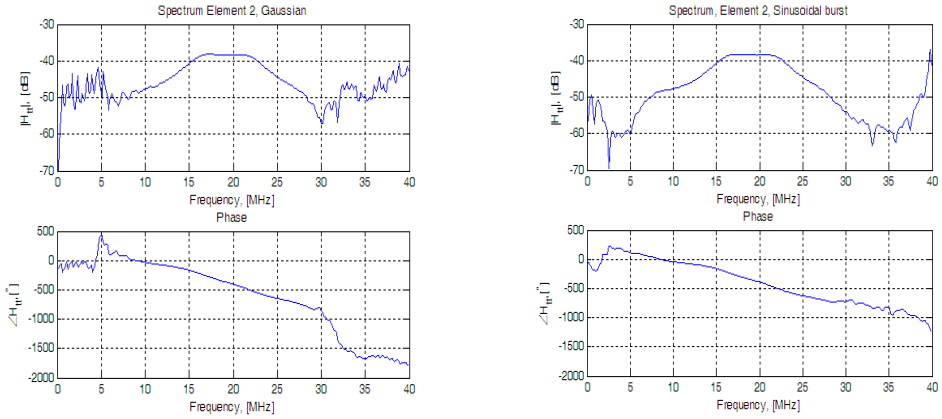

(a) H_{tt}, Gaussian (b) H_{tt}, sinusoidal

Figure 6.2: Complex electroacoustic transfer functions for element 2

By observing these figures more, it is clear that there is some noise and unwanted signals outside what seems to be the passband of the transfer functions, which is around 5-30 MHz for the sinusoidal excitations, and around 10-27 MHz for the Gaussian excitations for both elements. However, the fact that the amplitude of the transfer function tends upwards toward 40 MHz, especially for the sinusoidal excitations can be due to some aliasing effects that possibly have not been taken into account for.

The phase of the transfer function was found by approximating linearity. By taking data from two points in the plots, the total phase was then found as the calculated slope of the phase curve using the following relationship

$$\angle H_{tt} = \omega \tau_{tot} \tag{6.2}$$

where τ_{tot} is the total time delay of the system, where the electrical delay and water-path delay is included, mentioned in Chapter 6 and Chapter 7. The total time delay is then found by

$$\tau_{tot} = \frac{\Delta \angle H_{tt}}{\Delta \omega} \tag{6.3}$$

where the $\Delta \angle H_{tt}$ comes from the difference between two points of the phase plots, as these were as mentioned approximated to be linear, where $\Delta\omega = 2\pi \cdot \Delta f$. The Table 6.1 below gives an overview of the time delays approximated for element 1 and 2 for the different pulses.

The estimated values for the time delay is quite substantial, as the expected delay is half the period of the center frequency $0.5 \cdot \frac{1}{f_0}$, where f_0 is the center frequency of the transducer, as found in the simulations. With a center frequency of 20 MHz, the expected time delay therefore becomes 25 ns. We see that the delays calculated from the results are in the range 100 ns.

Table 6.1: The approximated time delays for the different pulses

Pulse type	Element nr	$\frac{\lvert\Delta\angle H_{tt}\rvert}{\Delta\omega}$, [ns]
Sinusoidal burst	1	91.7
Gaussian	1	103.2
Sinusoidal burst	2	96.0
Gaussian	2	145.5

This is quite a deviation from what was expected. However, the shape and trend of estimated phase of the transducer transfer function seem to coincide quite well with the simulated value. Both the simulated and the experimentally estimated phase has a transition from positive to negative values around 10 MHz. A positive phase value is not desirable, as this doesn't make sense physically.

Butterworth, Chebychev and Elliptic filters were used on the signals in the expression for the transfer function in Equation (3.9), but these did not improve the amplitude characteristics of the transfer function, sometimes even giving higher noise levels on the sides of the transfer functions. Introducing filters also distorted the phase information of the electro acoustic transfer function, so the use of filters was not pursued further for this parameter.

6.2 Reflection Coefficients of the Transducer

The reflection coefficients obtained for element 1 and element 2 of the transducer array, using a sinusoidal burst pulse, and a Gaussian pulse is given. The figures give the reflection coefficients obtained at different distances between the transducer and the reflector, in order to find the distance giving the best results for the reflection coefficients. All the plots of the reflection coefficients in general are colour coded, where the blue plot is the relation between the second and the first echo, $R_{T,2,1}$, the red plot is $R_{T,3,2}$ and the black plot is $R_{T,4,3}$.

6.2.1 Results from Element 1

To start with, the reflection coefficients at different depths, the pulses corresponding to the optimal depth and the frequency spectra of these pulses are given for element 1, where a Gaussian burst pulse was used to excite the transducer.

Gaussian pulses

Below are the results obtained when exciting the transducer with a Gaussian burst puls described more in detail in Chapter 5.

It can be observed that the best results are for the 2.05 mm distance between the transducer and the reflector. The following echoes for this depth and their corresponding frequency spectra in Figure 1 shows the echoes taken at the optimal position, and is given in the appendix I. The spectra are shown in Figure 6.5.

These pulses were unfiltered, only their DC component had been removed. By observing the curves for the reflection coefficients it is clear that there is mostly noise dominating in the region below 10MHz, this can be due to reflections from surrounding surfaces including the periphery of the reflector in contact with water. One important thing to be pointed out here is the fact that low frequency ultrasonic ultrasonic signals undergo relatively less attenuation than the high frequency ultrasonic signals. This means that the low freqency signals can survive multiple reflections and longer propagation distances. The Reflection coefficient $R_{T,2,1}$

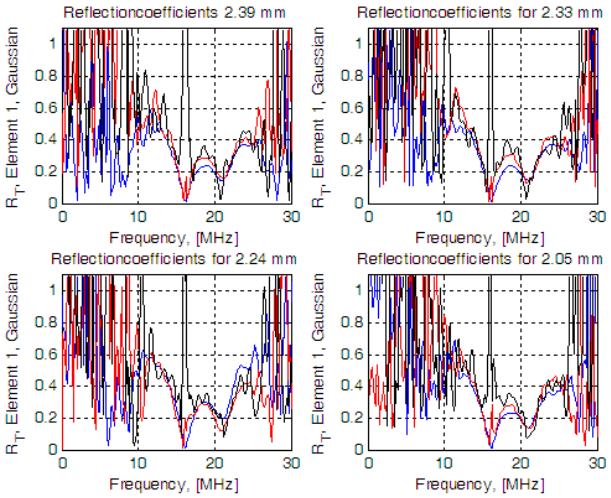

Figure 6.3: The reflection coefficients, element 1, Gaussian burst pulses 2.05-2.39mm distance from transducer to reflector

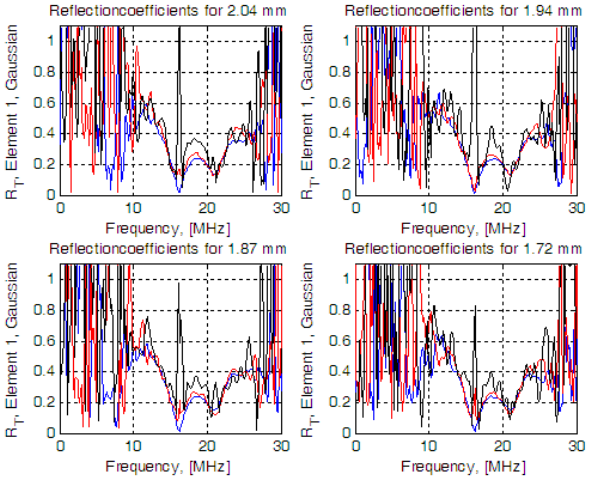

Figure 6.4: The reflection coefficients, element 1, Gaussian pulses 1.72-2.04mm distance from transducer to reflector

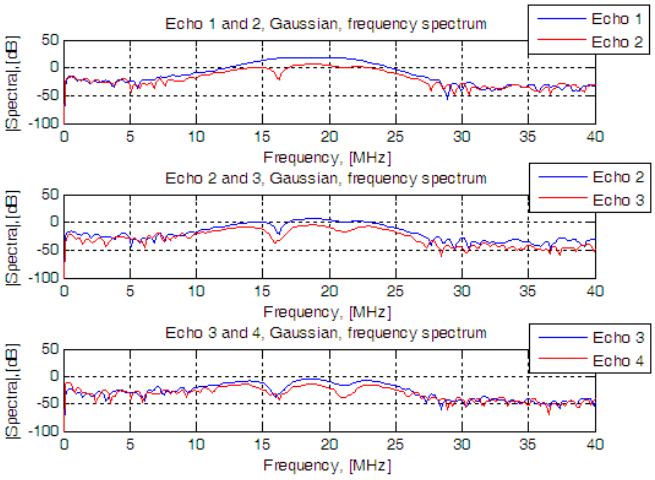

Figure 6.5: The frequency spectra for the echoes for Gaussian pulses

goes toward 0 at approximately 16MHz. A reflection coefficient that is 0 means that there are no internal reflections inside the transducer, meaning that there is a maximum of transfered power. In this case it means that there is a maximum transfer of electrical to mechanical energy at 16 MHz. It is also expected that the reflection coefficients follow one another in form, as it is the same signal being reflected back and forth. If the reflection coefficients do not have the same trend, it can be due to spurious reflections from other surfaces. The reflection coefficients are observed to follow the same trend to some degree in the region of interest, which is from 10MHz to 30MHz. It is also seen that there is a slight deviation of height between the reflection coefficients in the frequency range of interest, where the largest deviation closest to 20 MHz was measured at 18.55 MHz to be $R_{T,4,3} - R_{T,3,2} = 0.08$, $R_{T,4,3} - R_{T,2,1} = 0.1255$ and $R_{T,3,2} - R_{T,2,1} = 0.0455$. By observing the frequency spectra for the echoes, a sudden dip in the amplitude characterisitics can be seen at 16 MHz for echo 2, while this dip occurs somewhat earlier for echoes 3 and 4, but echo 4 is slightly higher than echo 3 at exactly 16 MHz. The sudden dip at echo 2 can explain the similar sudden dip observed above in the reflection coefficient $R_{T,2,1}$ corresponding to the Gaussian pulse in Figure 6.3. A sudden dip at a certain frequency means that there is minimal energy of the signal at that particular frequency. This also explains that there is a minimal reflection at 16 MHz, as perhaps the pulse is too low to be able to reach the reflecting boundaries within the layers of the transducer, as it possibly gets attenuated before it reaches the boundaries.

Sinusoidal Burst Pulses

Below in Figures 6.6, 6.7, 2, 6.8 are the similar results for the sinusoidal burst pulse, where no filtering has been done, except for the removal of the DC component of the pulses. We can again see that the range of interest is from 10MHz to 30MHz, and again, we observe a sudden dip at 16 MHz for echo 2. However, there is a substantial amount of noise outside the frequency range 10-30 MHz.

With 2.39 mm distance between the transducer, the corresponding frequency spectra shown in Figure 6.8 are obtained. The corresponding echoes are given in the appendix I.

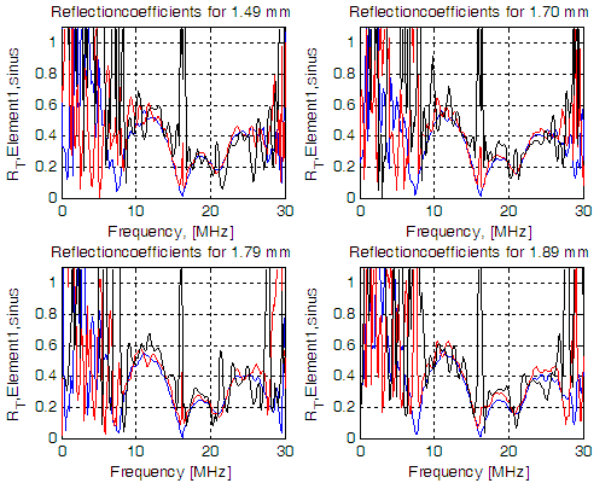

Figure 6.6: The reflection coefficients, element 1, sinusoidal burst pulses 1.49-1.89mm distance between transducer and reflector

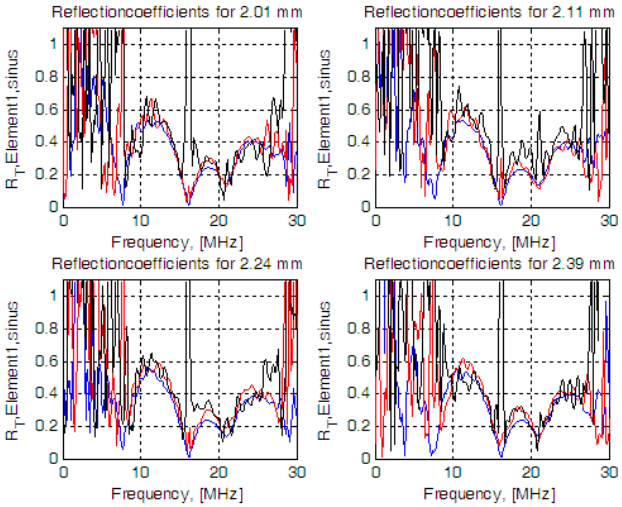

Figure 6.7: The reflection coefficients, element 1, sinusoidal burst pulses 2.01-2.39mm dustance from transducer to reflector

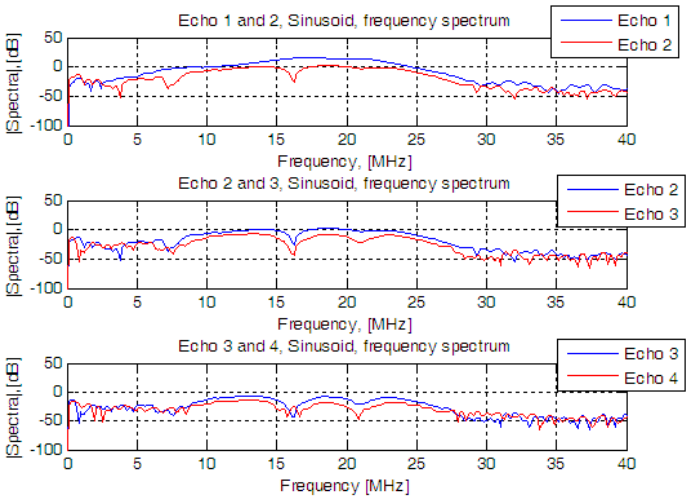

Figure 6.8: The frequency spectra for the sinusoidal burst pulses, element 1

6.2.2 Results from element 2

Similar measurements were also done on element 2 of the transducer array, and the following results were obtained.

Gaussian pulses

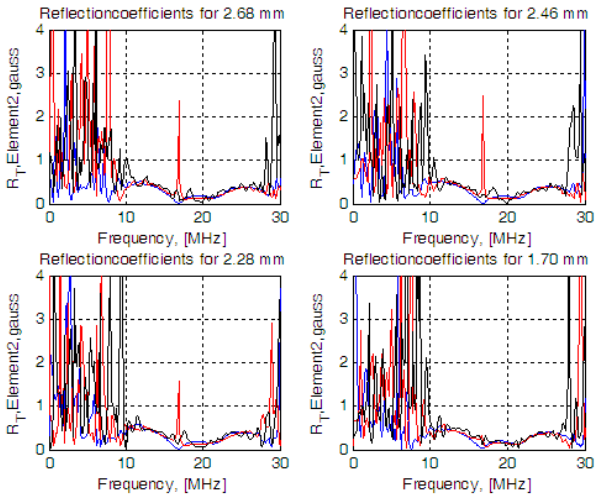

Figure 6.9: The reflection coefficients, element 2, Gaussian burst pulses 1.70-2.68mm distance between transducer and reflector

The 2.09 mm distance between the transducer and the reflector was found to be the best, giving the following frequency spectra shown in Figure 6.11. The corresponding echoes are given in 3 in appendix I

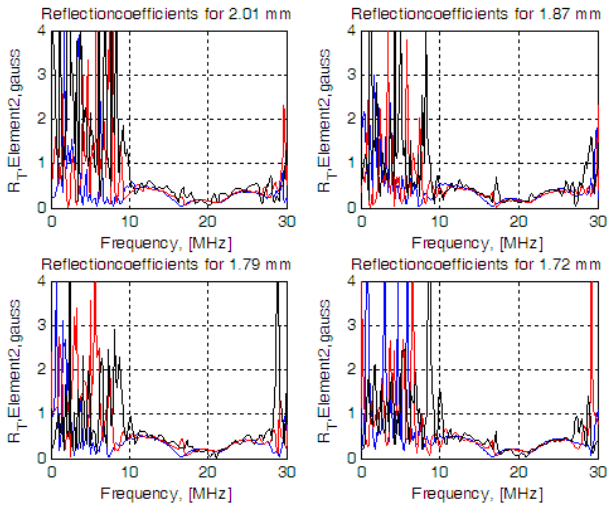

Figure 6.10: The reflection coefficients, element 2, Gaussian pulses, 1.72-2.01mm distance between transducer and reflector

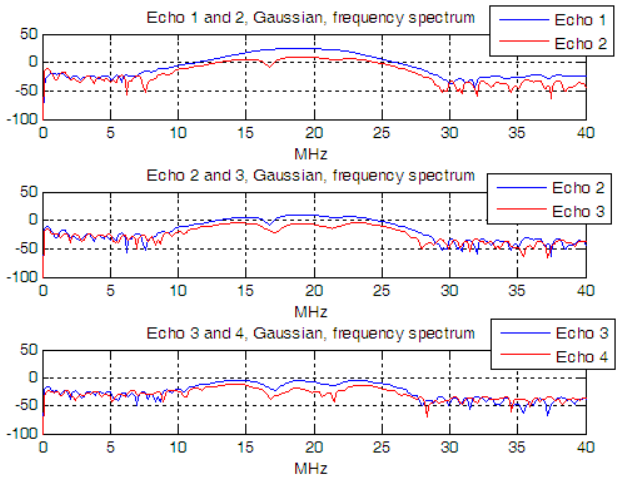

Figure 6.11: The frequency spectra of the pulses found in Figure 3

Table 6.2: The difference in optimal distance for the different elements and pulses

Pulse Type	$\lvert\Delta d_{element}\rvert$, [mm]	Δd_{pulse}, [mm]
Gaussian	2.39-2.05=0.34	2.26-2.05=0.21
Sinusoidal	2.26-2.09=0.17	2.39-2.26=0.13

Similarly as for element 1, the reflection coefficients obtained when exciting the transducer with a sinusoidal burst pulse is found for different depths.

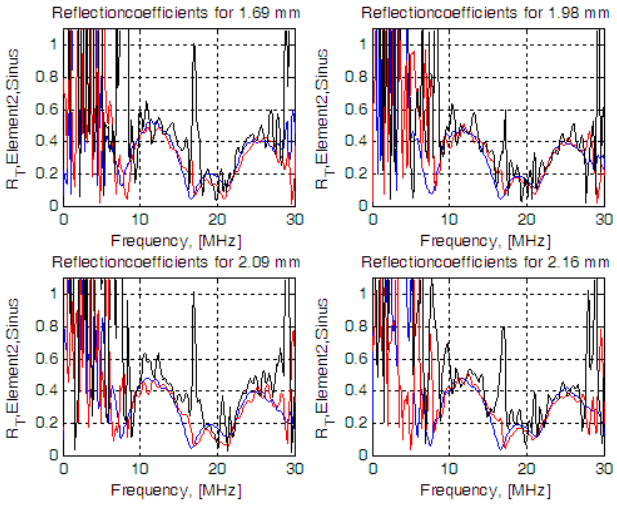

Figure 6.12: The reflection coefficients, element 2, sinusoidal burst pulses 1.69-2.16 mm from transducer to reflector

The 2.26 mm distance between the transducer and the reflector was found to be the best, giving the following frequency spectra shown in 6.14 and their corresponding echoes are given in Figure 4 in appendix I.

The general observation is that the reflection coefficients are optimal for different distances between the transducer and the reflector. This can also be due to uncertainties involved in measuring the distance between the transducer and the reflector using time considerations. However, it can also be due to deviations in the placements of foci of the elements. There can be a slight deviation of focus points for the different elements when the elements are arranged in an array, even though elements 1 and 2 are specified to have the same depth of focus. When comparing the optimal distances obtained for element 1 with the sinusdoidal burst pulse and the Gaussian pulse, we see a difference of distance 0.34mm. In element 2, the difference between the best distances between the transducer and the reflector obtained for the Gaussian excitation and the sinusoidal excitations is 0.17 mm. Table 6.2 below shows the best distances found for the different pulses and elements, and gives an idea of the difference between the best distances with respect to the reflection coefficients, where $\Delta d_{element}$ gives the difference between the distances found for the different elements of the same pulse type, and Δd_{pulse} gives the the difference between the distances found for different pulse types for the same element.

The increment in the depth scans were from approximately 0.1 mm to 0.15 mm. From this it can be seen that the optimal distance between the transducer and the reflector is varying to some extent with the different pulses and elements.

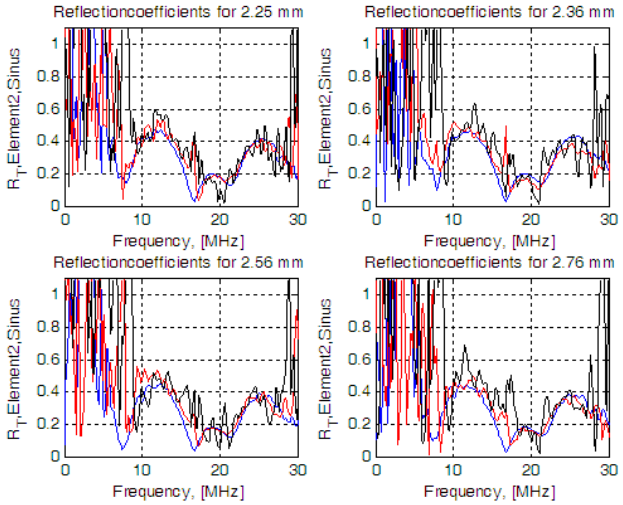

Figure 6.13: The reflection coefficients, element 2, sinusoidal burst pulses 2.25-2.76mm from the transducer to the reflector

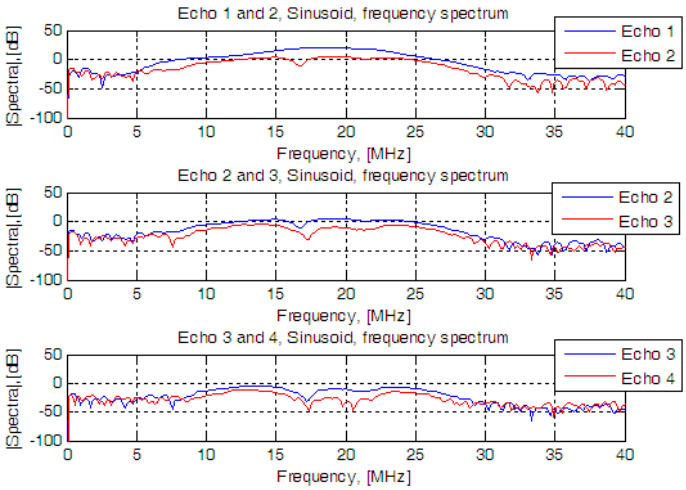

Figure 6.14: The frequency spectra of the pulses found in Figure 4

Table 6.3: The different filters used with their coefficients

Pulse	Element nr.	Filter	$m_{R_{2,1}}$	$m_{R_{3,2}}$	$m_{R_{4,3}}$
Sinus burst	1	Butterworth, order 2	1.0615	0.2398	0.0444
Sinus burst	1	Chebychev (II), order 1	0.4689	0.1223	0.0148
Sinus burst	1	Chebychev (I), order 2	0.9467	0.2159	0.0449
Sinus burst	1	Elliptic, order 2	0.9467	0.2158	0.0320
Gaussian	2	Butterworth, order 2	8.7232	1.0377	0.1395
Gaussian	2	Chebychev (II), order 2	4.0815	0.5396	0.0860
Gaussian	2	Chebychev (I), order 2	4.2471	0.5608	0.0893
Gaussian	2	Elliptic, order 2	4.7133	0.6228	0.1217
Sinus burst	2	Butterworth, order 2	1.8073	0.2776	0.0476
Sinus burst	2	Chebychev (II), order 1	0.7417	0.1295	0.0287
Sinus burst	2	Chebychev (I), order 2	1.6106	0.2506	0.0650
Sinus burst	2	Elliptic, order 2	1.3422	0.2504	0.0540

6.3 Reflection Coefficients with Filtering

In order to get improved quantities, where the coefficients followed the same trend to a greater extent than what was found using unfiltered signals, some filtering techniques were applied to the rf data of the echo signals in the fourier domain. This was also done to remove the unwanted noise outside the range 10-30 MHz. The different filters used were Butterworth, Chebychev type (I) and type (II) and Elliptic filters. In addition to this, a type of Wiener filtering has also been applied. A true Wiener filtering has not been done but an appropriate constant has been added to the denominator of the expression for the reflection coefficient as used in MATLAB, shown below in Equation (6.4), in order to cut the noise outside the pass band of 10-30 MHz from a certain value, as shown in Figure 6.15.

$$\frac{V_{n+1} \cdot {V_{n,filtered}}^*}{{V_{n,filtered}}^2 + m} \cdot \frac{1}{R_{wb} \cdot \alpha^2} \tag{6.4}$$

Where $*$ is the conjugate, and α and R_{wb} are given in Equation (5.8). V_n and V_{n+1} are the Fourier transforms of the rf data for the recorded echoes, n is the echo number and m is the constant in the denominator of Equation (6.4), where it was calculated in MATLAB as the maximum of $V_{n,filtered}$ squared divided by a constant γ which was found individually for all the reflection coefficients for the different pulse types and elements [1]. An overview of the filters used for the sinusoidal burst excitations and the Gaussian excitations is given in Table 6.3, for element 1 and element 2.

The resulting plots for the different elements and pulses are given in the following sections.

6.3.1 Element 1

Gaussian pulse

When attempting filters on the signals used to obtain the reflection coefficients for the element 1 when using a Gaussian excitation, an opposite effect of what was expected was observed. The resulting reflection coefficients became worse, and $R_{T,2,1}$ lost it's original shape, and exceeded 1 at 23 MHz, when using a second order Butterworth filter on the signals. After trying various

[1] $m = max(V_{n,filtered})^2/\gamma$, where γ is a chosen constant

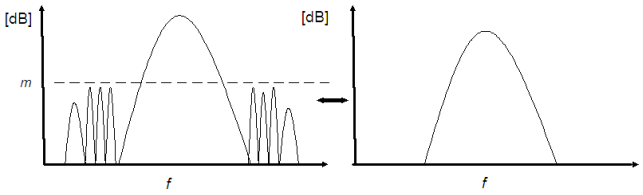

Figure 6.15: Effect of the modified Wiener filter

types and orders of filters on element one, including Elliptic and Chebychev filters and not getting a more desirable plot, filters were therefore discarded for element 1 for the Gaussian pulse.

Sinusoidal burst pulse

In order to eliminate as much noise as possible, different filters were used and they seemed effective in this case. The filters were used for the echoes in the expression for the reflection coefficient as used in MATLAB, given in Equation (6.4). Below in Figure 6.16, the reflection coefficients after doing a Butterworth filtering of order 2 is shown, and in the lower part of the window, the modified Wiener type of filter has also been applied.

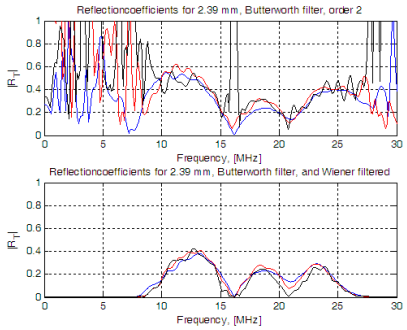

Figure 6.16: Effect of Butterworth second order filter, and modified Wiener filter

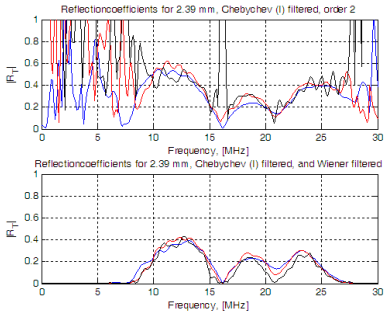

Figure 6.17: Effect of Chebychev (I), order 2 filter, and modified Wiener filter

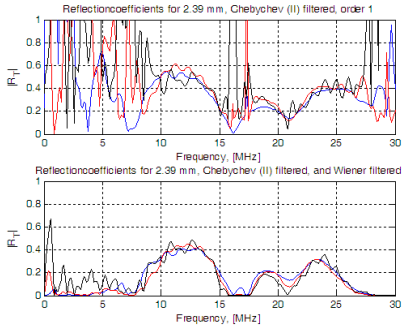

Figure 6.18: Effect of Chebychev (II), order 1 filter, and modified Wiener filter

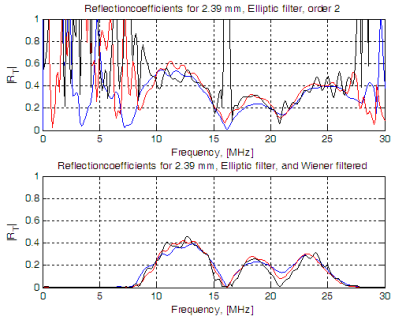

Figure 6.19: Effect of Elliptic, order 2 filter, and modified Wiener filter

It can be observed here that the modified Wiener type of filter has removed all signals from frequencies outside the range of 10 to 30MHz, as this was mainly noise, it made it easier to see the informative part of the plot. It has, however, also contributed to the fact that all the reflection coefficients for all the echoes were very close to zero at around 16 MHz, and hence some information was lost.

6.3.2 Element 2

Gaussian pulse

Filtering the echoes from the Gaussian excitation pulse on element 2 proved effective, opposed to element 1, using the same excitation. Figure 6.20, Figure 6.21, Figure 6.22 and Figure 6.23 all show the filtered reflection coefficients, where the filters are given in Table 6.3.

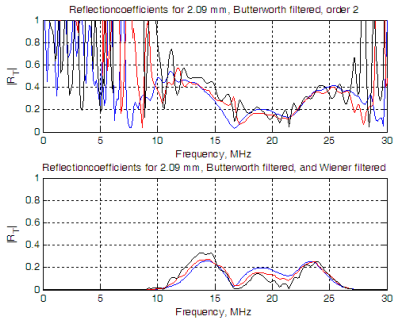

Figure 6.20: Effect of Butterworth, order 2 filter, and modified Wiener filter

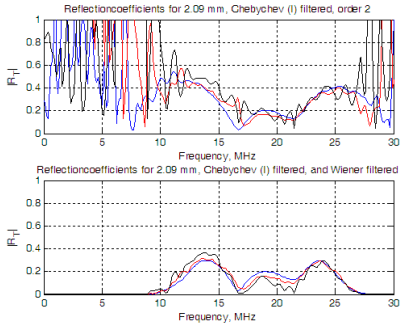

Figure 6.21: Effect of Chebychev (I), order 2 filter, and modified Wiener filter

Unlike the sinusoidal burst pulse in element 1, the gaussian pulse responded badly to a 2 order type (II) Chebychev filter, so a first order filter was used instead. It can be observed that the filtering led to that the reflection coefficient obtained between echo 4 and echo 3 is nearly reduced to zero at around 17 MHz.

Sinusoidal burst pulse

Filtering the echoes obtained with a sinusoidal excitation is found for the four different types of filters specified in Table 6.3, in Figure 6.24, Figure 6.25, Figure 6.26 and Figure 6.27.

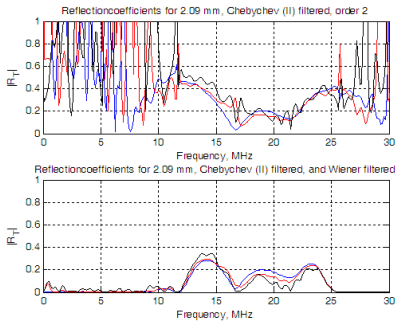

Figure 6.22: Effect of Chebychev (II), order 2 filter, and modified Wiener filter

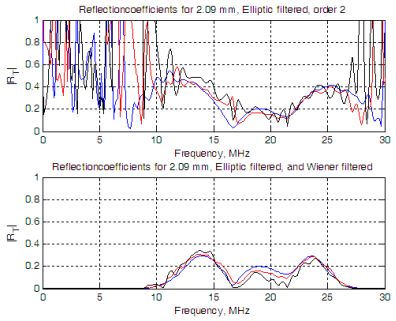

Figure 6.23: Effect of Elliptic, order 2 filter, and modified Wiener filter

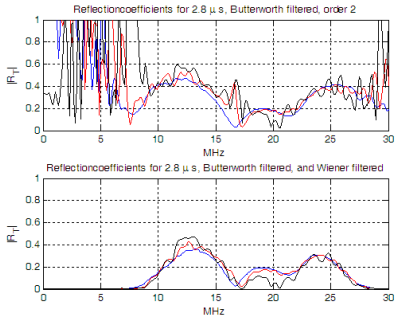

Figure 6.24: Effects of Butterworth, order 2 filter, and modified Wiener filter

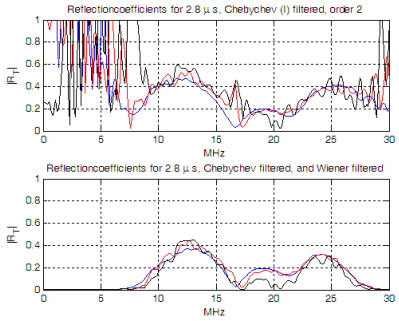

Figure 6.25: Effects of Chebychev (I), order 2 filter, and modified Wiener filter, Element 2, Sinusoidal

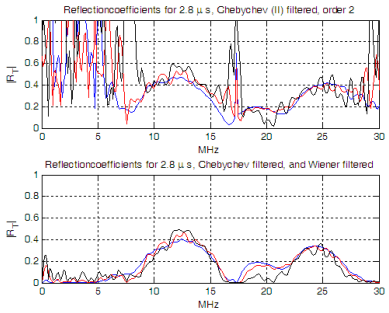

Figure 6.26: Effects of Chebychev (II), order 1 filter, and modified Wiener filter

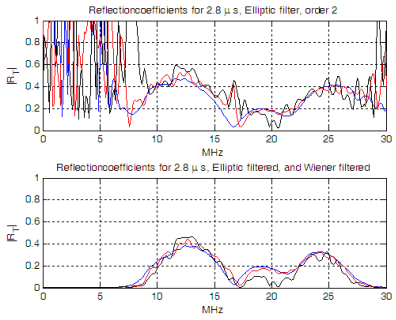

Figure 6.27: Effects of Elliptic, order 2 filter, and modified Wiener filter

6.3.3 Phase of the Reflection Coefficients

The phase of the reflection coefficients found between echo 1 and echo 2 is given in the Figure 6.28 below, in order to give an idea of how the phase looks like. This is the phase obtained after the waterpath in water was eliminated. As one can see, the phase characteristics of the reflection coefficients are not as linear as the phase characteristics for the transfer functions.

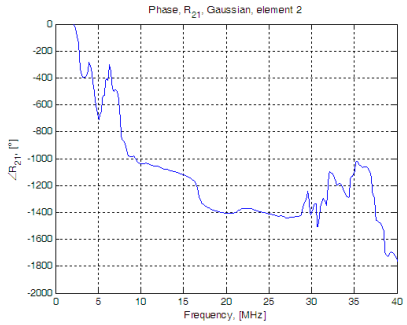

Figure 6.28: Reflection coefficient phase

Chapter 7

Measurement Errors and Discussion

7.1 Cabling Effects

Cabling has a considerable amount of influence on the performance of a high frequency system. Normal wires can distort the signals rather severely, so coaxial cables were chosen, as these are easier to control and have specified values as to how the cables might affect the system. The normal wires were cut shorter than they initially were, however, the results seem to indicate that they were not cut short enough, due to that an inductive value of 70 nH had to be subtracted from the system. In order to see the effect of the coaxial cables coming from the normal wires from the elements on the transducer, the impedance was measured at the end of the normal wires, at the array holder, and then at the connectors on the circuit board seen in Figure 4.4. We see that the coaxial cables contribute to an inductive value by looking at the phase characteristics, and the calculated value of the inductance due to the coaxial cable was found to be 40 nH in Chapter 6. Wires resembling the non coaxial cables were cut to the same length as the ones used in the set-up, and the 2.5 cm referance cable was then modeled as an LC circuit in the impedance analyzer to calculated the inductanctive value associated with such a cable. This gave a value of 20 nH. As the inductances are presumed to be in series, that leaves 10 nH as the inductive contribution of the wires inside the transducer.

7.2 Pulse Splitting

When observing the echoes from the reflector, some pulses were observed to be split and therefore stretched in time, especially echoes 2 and above. Factors contributing to the structure of echoes, for example the amplitude and shape of the echoes from major reflecting boundaries, is dependent on the pulsed nature of the emitted sound field. This can introduce complex variations in the echoes shapes, as mentioned in [12], where the echo structure in medical ultrasonic pulse echo scanning is discussed in detail, where the reflections are from tissue boundaries. Nevertheless, the principles can also be applied in this case. The importance of positioning of the transducer with respect to the reflector was discussed, as seen in Figure 7.2, and it was illustrated for a plane circular transducer, that splitting occured when the transducer and reflector were off axis compared to one another, and that the off axis echo was amplified with a factor of 10 relative to the axial echo, as seen in Figure 7.3. Lateral positioning was also found to be important here, as seen in Figure 7.4

Although this illustration was taken in the far field, and the transducer used by [12] were plane circular transducers, pulse splitting and pulse stretching due to positioning problems applies to many cases. This was was also observed in our experiments, when the transducer

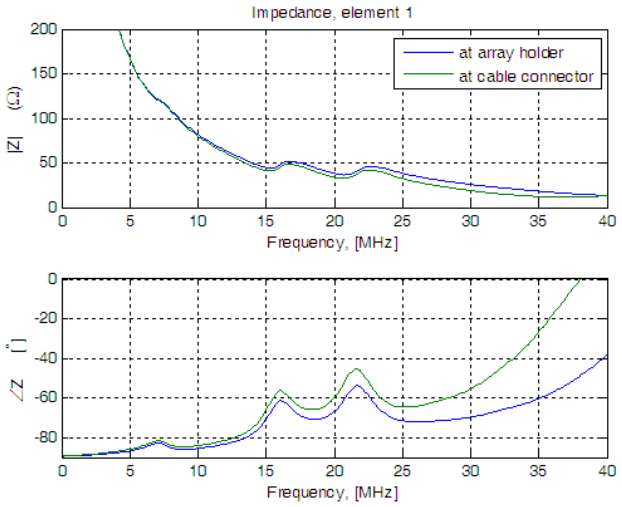

Figure 7.1: Effect of cabling on impedance measurements

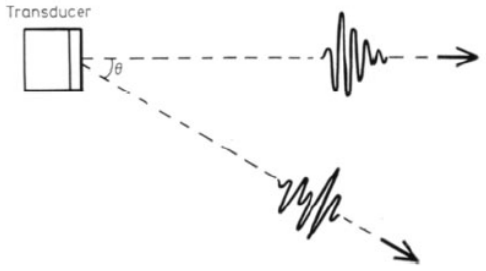

Figure 7.2: Illustation of how a pulse can be distorted if the positioning of the transducer with respect to the reflector is not right, [12]

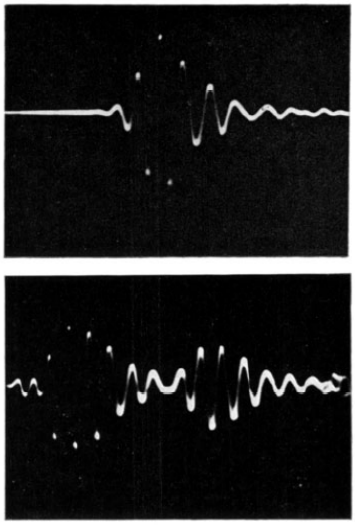

Figure 7.3: Pulse splitting in the field of a 2.5 MHz plane circular transducer, where the upper pulse was measured on axis, and the lower was measured 7mm off axis, and it was amplified with a factor of 10 relative to the axial pulse [12].

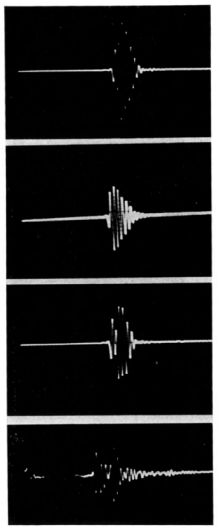

Figure 7.4: Variations seen in the echostructure from a plane disc reflector when laterally transversing the field of a 2.5 MHz plane circular transducer [12].

was not positioned in the optimal lateral position, as seen in Figure 7.5.

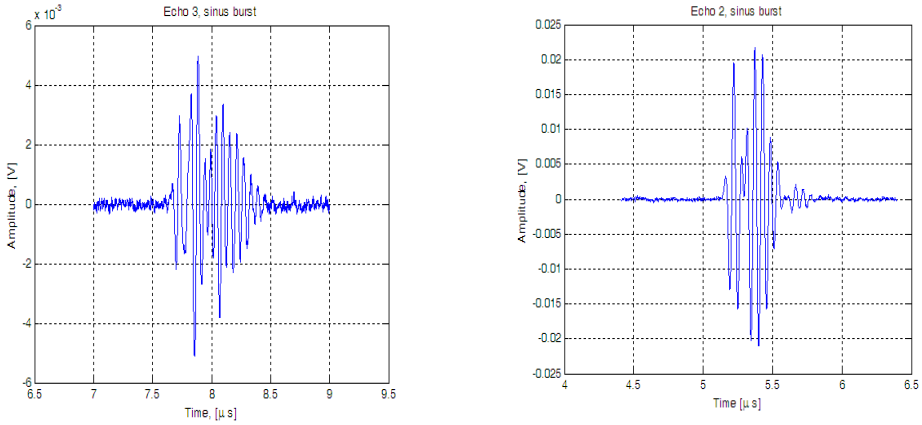

(a) Pulse splitting, Echo 2

(b) Pulse splitting, Echo 3

Figure 7.5: Pulse splitting with non optimal positioning

7.3 The Oscilloscope as a Component in the Set-up

Another valid issue is that the ocilloscope is an active component in the electrical transmission chain. This will also have an effect on the signal flow of the system. As it has a 50Ω impedance it cannot be ignored from the circuit, as power also will go into the oscilloscope. Initially, in [19], the oscilloscope had a coupling of 1MΩ, and results were achieved from this. However, if one analyzes the effect of high frequencies with the transmission line equation, one can see the following from the input impedance of the transmission line circuit

$$Z_{iscp} = Z_c \frac{Z_{sc} + jZ_c \tan kL}{Z_c + jZ_{sc} \tan kL} \tag{7.1}$$

Where Z_{iscp} is the input impedance seen looking from the cable into the oscilloscope, Z_{sc} is the parallellcoupling of 1MΩ and 10pF at the entrance of the oscilloscope, and Z_c is the cable impedance, set to be 50Ω. Where the oscilloscope is the load, and the impedance of the coaxial cable, Z_c is 50Ω. For $k = 2\pi/\lambda$ and $L = \lambda/4$, we see that Equation (7.1) simplifies to

$$Z_{iscp} = \frac{{Z_c}^2}{Z_{sc}} \approx 0 \tag{7.2}$$

This implies that there is effectively a short circuit at the oscilloscope input. Some of the results obtained when using 1MΩ can be explained by this effective short circuit experience at the oscilloscope input. When applying a 1MΩ coupling, it was observed that the echo plot on the oscilloscope had an upwards slanting time axis. When increasing the amplitude sensitivity for the channels, it was nearly impossible to aquire the signals, as the offset on the oscilloscope created difficulties to even locate the signal on the amplitude axis.

There are solutions to the problem of the influence of the scope in the electrical circuit. For example, one could

- Use a shorter cable between the pulse generator and the oscilloscope. This was tried, but the results weren't very impressive, so further investigations on this was not done.

- Set the scope coupling to 50Ω. This was done for the experiments done for this thesis, as this gave results without causing complications and delays due to redoing the set-up. By setting the oscilloscope coupling to 50Ω, impedance matching with the cable impedance Z_c was achieved.

- Another option would have been to have been to get a probe/measuring cable with an amplifier and couple it into the oscilloscope, as this would ensure that when looking into the circuit, only the amplifier would have been seen in input impedance considerations. In addition to this, the signal to noise ratio would be improved, as the signal would be stronger due to the amplifier. With the current set-up, this could have been done by cutting the coaxial cable with the MCX connectors in one end and the BNC connectors in the other end shown in Figure 5.4 and soldering an amplifier into the cable. This is certainly an interesting idea for future research. A suggestion to this is using a regular x10 probe.

7.4 Surrounding Noise and its Effects

When doing the experiments, there was at certain times observed a great deal of noise when tuning up the sensitivity of the oscilloscope and looking at the later echoes. The noise did not respond to switching the robot off, as the robot was known to contribute to quite a lot of noise. In some cases before finding the optimal position as was done when takig a 3dscan, the noise level nearly dominated over the signal level of the fourth echo, as shown in Figure 7.6. A theory is that the normal wires took up the noise, as the coaxial cables are well shielded. In order to investigate the possible noise isolation as an attempt to shield the normal wires, the bottom part of the transducer holder can be shielded with a metall coating in order to get similar effects of a coaxial cable. The noise in the laboratory varied generally from day to day, depending on which of the surrounding equipments were turned on, so an important note for further work would be to perhaps do these measurements in another noise free location, or to be sure that the electrical equipment in the laboratory is turned off when performing the experiments.

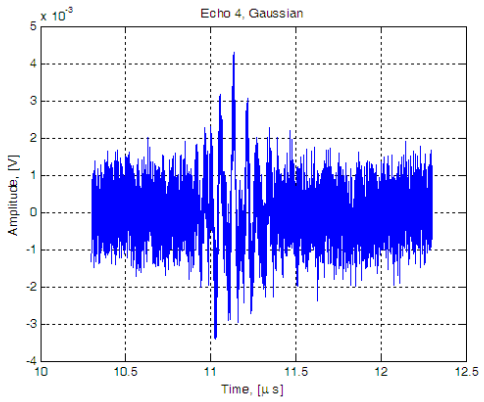

Figure 7.6: Measured Echo 4, where noise is dominating

7.5 Pulse Distortion at High Frequencies

Another interesting observation was that the sinusoidal burst pulses were to a certain extent distorted when a frequency of 20 MHz was used, as seen in Figure 7.7. This might be due to that the Arbitrary Waveform Generator possibly has some difficulties when transmitting high frequency burst pulses,as observed in Figure 7.7. Instead of giving a pulse of one period, some ringing is observed.

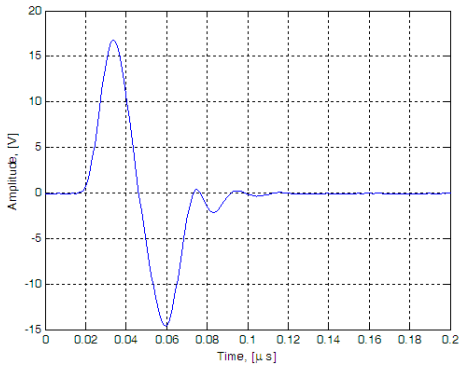

Figure 7.7: Distorted sinusoidal burst pulse, 20 MHz

7.6 Time Delay Compensation in Water

When calculating the time delay compensation in water, there are some accuracy demands that should be taken into consideration. The period of the pulse driven at $f_0 = 20$MHz, is 50ns. It is therefore important that the time measurement error is less than 50ns for the results to be accurate. A reasonable demand would be to have a 10° deviation corrosponds to a $\frac{1}{36}$ of a whole period resulting in a $\frac{50}{36} = 1.4$ns. The differing time windows of the recorded echoes and pulses are therefore significant in comparison to this number. Further investigation to obtain accurate quantities of the time delay may be vital for the phase information of the complex parameters.

7.7 Uncertainty

As this was an experimental set-up, measurement uncertainties have to be estimated to set the whole picture. An uncertainty budget of type B is made for the set-up, meaning that an analysis based on the underlying uncertainties of the equipment is taken account for in the measurements, [18]. Table 7.1 gives the uncertainties of the instruments used in the measurements.

The logarithmic differentiation expressions for the electro acoustic transfer function H_{tt} and the reflection coefficients R_T both use the equations defining these parameters, given in Equation (3.9) and Equation (5.8) respectively, by defining the uncertainty in each of the components in the equations. Equation (7.3) and Equation (7.4) give the logarithmic differentials for the amplitudes of the electro acoustic transfer function and the reflection coefficients respectively, where $d|H_{tt}|$ is the differential for the electro acoustic transfer function and $d|R_T|$ is the differential for the reflection coefficients.

Table 7.1: Uncertainties in the instruments and derived parameters

Quantity	Measured	Instrument	Uncertainty	Derived
Z_{ri}	x	Impedance Analyzer	0.17% for Impedance	-
Z_r	x	Arb. Waveform Generator	1.0%	-
H_{ri}	-	-	-	x
H_{tt}	-	-	-	x
Z_L	-	$\pm 0.0005 \cdot 10^6$	x	
V_r	x	Oscilloscope	2% and 1.5%	-
V_{tt}	x	Oscilloscope	2% and 1.5%	-
A	-	$0.005 \cdot 10^{-}3$	-	

$$2\frac{d|H_{tt}|}{|H_{tt}|} = \frac{d|V_r|}{|V_r|} - \frac{d|Z_L|}{|Z_L|} - \frac{dA}{A} - \frac{d|V_{tt}|}{|V_{tt}|} - \frac{d|H_{ri|}}{|H_{ri|}} \tag{7.3}$$

In the expression for the logarithmic differential of the reflection coefficient, the attenuation α is assumed to be constant, and therefore eliminated from the Equation (7.4) for the sake of simplicity, giving the following expression

$$\frac{d|R_T|}{|R_T|} = \frac{d|V_{n+1}|}{|V_{n+1}|} - \frac{d|V_n|}{|V_n|} \tag{7.4}$$

By taking the square root of the sum of squares of Equation (7.3) and (7.4), the following expressions are found

$$\frac{d|R_T|^2}{|R_T|^2} = \frac{d|V_{n+1}^2|}{|V_{n+1}^2|} + \frac{d|V_n^2|}{|V_n^2|} \tag{7.5}$$

finally giving the expression for the uncertainty of the reflection coefficient u_{R_T} as

$$u_{R_T} = [R_T^2(\frac{u_{V,n+1}^2}{u_{V,n+1}^2} + \frac{u_{V,n}^2}{u_{V,n}^2})]^{1/2} \tag{7.6}$$

and the uncertainty of the transfer function amplitude is given as

$$u_{H_{tt}} = [|H_{tt}|(\frac{du_r^2}{4V_r^2} + \frac{u_{ZL}^2}{4Z_L^2}) + \frac{u_A^2}{4A^2} + \frac{u_{Vtt}^2}{4V_{tt}^2} + \frac{u_{Hri}^2}{4H_{ri}^2}]^{1/2} \tag{7.7}$$

For finding errors in the phases of the complex parameters, the parameters are expressed in polar form. H_{ri} is then given as

$$H_{ri} = (Z_{ri}Z_r)(Z_{ri} + Z_r) = X_{ri} + jY_{ri} = |H_{ri}|e^{j\theta_{ri}} \tag{7.8}$$

giving the following expression for dH_{ri}

$$d|H_{ri}|/|H_{ri}| = \frac{X_{ri}^2}{X_{ri}^2 + Y_{ri}^2}(dX_{ri}/X_{ri}) + \frac{Y_{ri}^2}{X_{ri}^2 + Y_{ri}^2}(dY_{ri}/Y_{ri}) \tag{7.9}$$

similarly $d\theta_{ri}$ can be found as

$$d\theta_{ri} = \frac{X_{ri}dY_{ri} - Y_{ri}dX_{ri}}{X_{ri}^2 + Y_{ri}^2} \tag{7.10}$$

These equations are equivalent to the following

$$\frac{d|H_{ri}|}{H_{ri}} = \cos^2(\theta_{ri})(dX_{ri}/X_{ri}) + \sin^2(\theta_{ri})(dY_{ri/Y_{ri}}) \tag{7.11}$$

$$d\theta_{ri} = \cos\theta_{ri}\sin\theta_{ri}(dY_{ri}/(Y_{ri}) - dX_{ri}/X_{ri}) \tag{7.12}$$

The similar relations given in Equation (7.10) and Equation (7.11) are given for $\frac{d|V_r|}{V_r}$ and $\frac{d|V_{tt}|}{V_{tt}}$.

The values of the parameters dX_{ri}/dX_{ri},dX_r/dX_r and dX_{tt}/dX_{tt} are all found by using practically sound assumptions using the manufacturers specifications and based on the values given in Table 7.1, giving a conservative estimate of these values.

The expression for the electro acoustic transfer function H_{tt} therefore becomes

$$H_{tt} = \frac{1}{\sqrt{2AZ_L}}\sqrt{\frac{|V_r|}{|V_{tt}|}}\frac{1}{|H_{ri}|}e^{j(\theta_r/2-\theta_{tt}/2-\theta_{ri}/2)} = |H_{tt}e^{j\phi_{tt}}| \tag{7.13}$$

where

$$\phi_{tt} = \theta_r/2 - \theta_{tt}/2 - \theta_{ri}/2 \tag{7.14}$$

With corrosponding differentials for θ_r and θ_{tt} based on the real and imaginary parts of V_r and V_{tt} given by $V_r = X_r + jY_r$ and $V_{tt} = X_{tt} + jY_{tt}$ and

$$d\theta_r = (X_r dY_r - Y_r dX_r)/(X_r^2 + Y_r^2) \tag{7.15}$$

similarly for $d\theta_{tt}$

$$d\theta_{tt} = (X_{tt}dY_{tt} - Y_{tt}dX_{tt})/(X_{tt}^2 + Y_{tt}^2) \tag{7.16}$$

The given relations above are then inserted into the expression for the transfer function's amplitude differential expression given above in Equation (7.3).

The errors in the amplitude values for the reflection coefficients and the transfer functions are given below in Figure 7.9 and Figure 7.8. It can be seen that the errors are very small for the reflection coefficients in the regions that aren't distorted by noise. This can also be because the reflection coefficients are amplitude values. The error for the transfer function gives a band of approximately 10dB around 20 MHz.

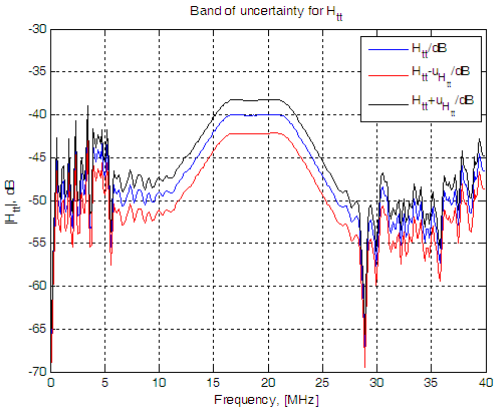

Figure 7.8: The uncertainty plot for $|H_{tt}|$

The errors in the phase of the transfer function is also given in Figure 7.10 and 7.11

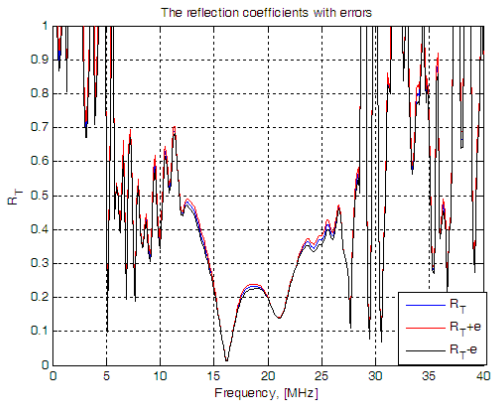

Figure 7.9: $|R_T|$ with uncertainty band

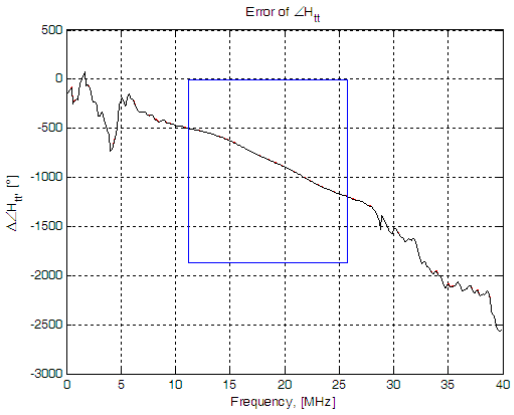

Figure 7.10: Phase uncertainty of H_{tt}, with zooming window

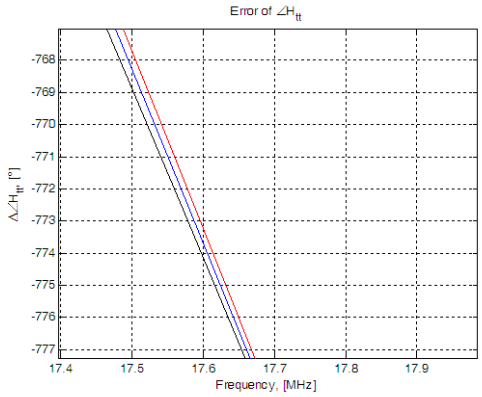

Figure 7.11: The phase error of H_{tt} using zooming window in Figure 7.10

It can be observed that the phase error due to the uncertainty contributions from the equipment is not dominant, as seen in the Figures above. This indicates that the big difference between the simulated phase of the transfer function and the experimentally aquired phase is due to some error in the estimation scheme. The delay found for the electrical transmission chain transfer function H found in Chapter 6 was found to be minor. Further investigations as to phase deviation due time delay considerations should therfore be performed. The system accuracy essentially boils down to the accurate determination of the time delays involved for the pulses considered for the estimation of the transfer function.

Chapter 8

Conclusion

8.1 General conclusion

An instrumentation and measurement set-up for characterization of an ultrasonic transducer has been developed, by constructing a reflector to give maximum echoes and reflection from its surface, and by designing a transducer holder that fulfills mechanical requirements of transducer alignment and electrical requirements of more control over the electrical signal propagation. The reflection coefficients and electro acoustic transfer function are estimated, as these combined with the electrical impedance of the transducer can fully characterize the transducer. The reflection coefficients only gave plausible values from a frequency band of 10-30 MHz, the estimated signal outside this band was mainly noise. The measured values agreed to some extent with the simulated values, although a big deviation in time delay for the electro acoustic transfer function was observed. This should be investigated further. Emphasis on developing a repeatable method to characterize the transducer by finding the reflection coefficients and electro acoustical transfer function has been done by characeterizing element 1 and element 2 of the transducer array, so that the same measurements and instrumentation can be repeated for all the other elements, though different reflectors should be used for element 6-8. Different types of filters were used to improve the results of the reflection coefficient, and the best parameters for the filter algorithms used were found. Positioning turned out to be vital to get good values for the reflection coefficients, so great care must be taken in finding the optimal position of the transducer with respect to the reflector. The optimal distance between the transducer and the reflector differed for the various excitations types and the different elements, some deviating from the expected distance of 2.12 mm, calculated using the focal depth of the transducer elements and radius of curvature of the reflector. The electro acoustic transfer function also agreed to some extent with the simulations, but the amplitude characteristics were more bandwidth limited than the simulated values, and there seemed to be effects indicating aliasing, which should perhaps be investigated further. The instruments used in the measurements were found to give a reasonable amount of uncertainty in the amplitude characteristics of the estimated parameters, giving mimimal errors in the reflection coefficients and an uncertainty band of 20dB for the electro acoustic transfer function.

8.2 Further Work

In this project, measurements have mainly been taken on element 1 and element 2 of the 8-element array transducer. In order to fully characterize the array, similar measurements and analysis should be done for all the elements. However, as element 6-8 all have a different

radius of curvature, these should have individual reflectors constructed with the same radius of curvature as each of these elements. Noise control is also an important issue that should be looked more into, as the noise in the present surroundings of the laboratory was quite substantial. Better electromagnetic screening of the non-coaxial cables in the system could be an idea to decrease the noise. More sensor based control of the actual distance between the transducer and the reflector would also be useful, as timedelay considerations between two consecutive pulses indicated some errors in the estimated distance. This was mainly due to noise, as reading the start of each pulse brought a certain amount of uncertainty and could be dependent on the individual taking the measurements. A more flexible mechanical fixture for the holder would also be useful, as this had to be frequently assembled and dismantled onto the robot. A knob device would perhaps make the set-up more user friendly. The length of the holder can also be decreased as it becomes prone to vibrations with increasing length. In order to shorten the non coaxial cables even more, the depth of the transducer holder can be reduced, as the deeper the holder is, the longer the non coaxial wires are. A metallic shielding for the area where the non coaxial cables are can also be tried, as this can potentially reduce the noise these cables tend to pick up. The oscilloscope as a component in the set-up is also an issue that should be adressed. Using probes with built in amplifiers makes the oscilloscope superfluous at the same time giving a stronger signal. With the given set-up, using the coaxial cables with MCX and BNC connectors on each end, this can be done by soldering an amplifier into the cable. Better control and quantification of the non coaxial cables is also an important measure to make the transmission line model as accurate as possible. While quantifying the effects from the outer non coaxial cables is important, a better analysis of the wires inside the transducer array itself should also be done in order to account for all the cabling effects in a more accurate way. By compensating for all the cables and components in the electrical circuit leading to the transducer ports, the electrical impedance can for example be determined to a better degree of accuracy at the transducer ports, and this quantity can help determine other parameters that can characterize the transducer, like the admittance and the electroacoustical transfer function, [24]. An interesting and important parameter that follows naturally from the reflection coefficients and the electroacoustic transfer function is the mechanical admittance, a component in the multiport structure matrix for the transducer that with the electrical impedance and electro acoustic transfer function can fully characterize the transducer, hence giving the user freedom to decide which load to give the transducer. Finding this parameter is a natural way of following up and completing the aims of the work done in this project.

For multi element arrays with a large number of elements [1], the design and measurement setup can be tedious, as this means that each element should be measured manually. In multi element cases with a high number of elements, field programmable gate arrays (FPGA)/field programmable analog arrays (FPAA) can be of use, as the user or designer of the transducer can specify certain characteristics beforehand, as for example the amplitude and phase characteristics of the transducer, where these quantities are specified to lie within a certain band while performing characterization experiments. When the characteristics of an element falls out of the band, the FPGA/FPAA can be programmed to adjust the characteristics to lie within the desired band. A more varied use of different pulses could also be interesting for further work, for example the use of a sinusoidal modulated pulse with a long period, could be interesting, as the frequency spectrum of this pulse has peaks at specified frequencies. As this pulse is very narrow banded, a lot of information around the specified frequency can be obtained, and by shooting pulses with peaks from a range of 10-40 MHz, a discrete pointwise value for reflection coefficients and transferfunctions within the frequency range can be obtained.

[1] in example 128 elements

Bibliography

[1] American Society for Testing ASTM and Materials. *Ultrasonic Testing, Attenuation in water as a function of frequency.* www.astm.org, 09.06.2007.

[2] B.A and Hans G. Torp. *Forelesningsnotater TTK4160/TTK4165 Høst 2003.* Department of Circulation and Medical Imaging, NTNU-Trondheim, April 30, 2000.

[3] The Free Dictionary by Farlex. *Atherosclerosis.* http://medical-dictionary.thefreedictionary.com/atherosclerosis, 22.06.2007.

[4] Stanislav Emelianov. *Medical Ultrasound: from imaging to drug delivery to survey.* http://www.engr.utexas.edu, 04.07.2007.

[5] C. Hu et al. Fpga based digital high frequency beamformers for arrays. *IEEE Ultrasonics Symposium*, 2004.

[6] E. Lacaze et al. 20 mhz ultrasound array for medical imaging :: From design to image evaluation. *IEEE Ultrasonics Symposium*, 2001.

[7] F.S. Foster et al. Principles and applications of ultrasound backscatter microscopy. *IEEE TRANSACTIONS ON ULTRASONICS, FERROELECTRICS, AND FREQUENCY CONTROL, Vol.40*, (5), September 1993.

[8] M. Vogt et al. Development of a high frequency ultrasound skin imaging system: Optimalization ultilizing time domain reflectometry and network analysis. *IEEE Ultrasonics Symposium*, 2003.

[9] M.E. Frijlink et al. Intravascular ultrasound tissue harmonic imaging in vivo. *IEEE Ultrasonics Symposium*, 2004.

[10] S. Fath. Experimental estimation of electro-acoustic transfer parameters for piezoelectric ultrasound transducers. May 25th, 2004.

[11] Dept. of Chemistry Frostburg State University Fred Senese. *Water Properties Calculator.* http://antoine.frostburg.edu/chem/senese/101/, 10.06.2007.

[12] J.C. GORE and S. LEEMAN. Echo structure in medical ultrasonic pulse-echo scanning. *PHYS. MED. BIOL*, 22(3):431–443, 1977.

[13] D.A. Christopher G.R. Lockwood, D.H. Turnbull and F.S. Foster. Beyond 30 mhz, applications of high-frequency ultrasound imaging. *IEEE ENGINEERING IN MEDICINE AND BIOLOGY*, November/December 1996.

[14] K. Hiltawsky. *Fortschritte in der Ultraschallbildgebung.* GE - Global Research Europe Imaging Technologies, 18.06.2007.

[15] HyperPhysics. *Piezoelectric effect.* http://hyperphysics.phy-astr.gsu.edu/hbase/solids/piezo.html, 10.12.2006.

[16] A. B.Coppens J. V. Sanders L. E. Kinsler, A. R.Frey. *Fundementals of Acoustics.* Wiley, Fourth Edition.

[17] G. Gonzales L. Medina, E. Moreno and L. Leija. Circular ultrasonic transducer characterization: theoretical and experimental results. *REVISTA MEXICANA DE FÍSICA*, 2003.

[18] National Physical Laboratory. *A Beginner's Guide to Uncertainty of Measurement.* http://www.npl.co.uk/publications, 20.06.2007.

[19] J. Mylvaganam. Instrumentation and measurement setup for characterizing high frequency piezoelectric ultrasound transucers. December, 2006.

[20] Olympus NDT. *Technical Notes.* www.olympusndt.com, 18.05.2007.

[21] National Institute of Biomedical Imaging and Bioengineering. *Resource on Medical Ultrasonic Transducer Technology.* http://www.nibib.nih.gov/, 18.06.2007.

[22] University of Purdue. Pulse echo system. 13.11.2006.

[23] J.M. Smith P.G. Kenny, J.J. Gruber. Ultrasonic transducer characterization. *Materials Evaluation*, (45), June 1987.

[24] A.L. Lopéz Sánchez and L.W. Schmerr Jr. Determination of an ultrasonic transducer's sensitivity and impedance in a pulse-echo setup. *IEEE TRANSACTIONS ON ULTRASONICS, FERROELECTRICS, AND FREQUENCY CONTROL*, 2006.

[25] L.W. Schmerr T.P Lerch and A.Sedov. Characterization of spherically focused transducers using an ultrasonic measurement model approach. *Res Nondestr Eval*, 1996.

[26] Iowa State University. *The System Function.* http://www.iastate.edu, 09.2006.

[27] J. Nelson Wright. *Image Formation in Diagnostic Ultrasound.* IEEE International Ultrasonics Symposium Short Course, 1997.

Part I

Appendices

Appendix

The echoes found at the optimal axial positions when performing a 3d-scan.

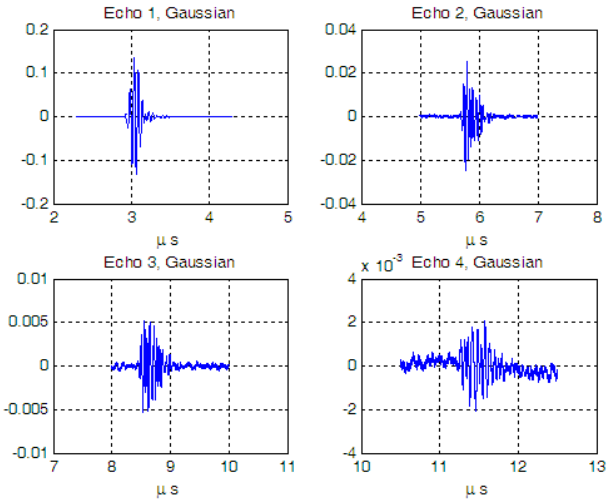

Figure 1: The echoes obtained with optimal positioning, element 1, Gaussian excitation.

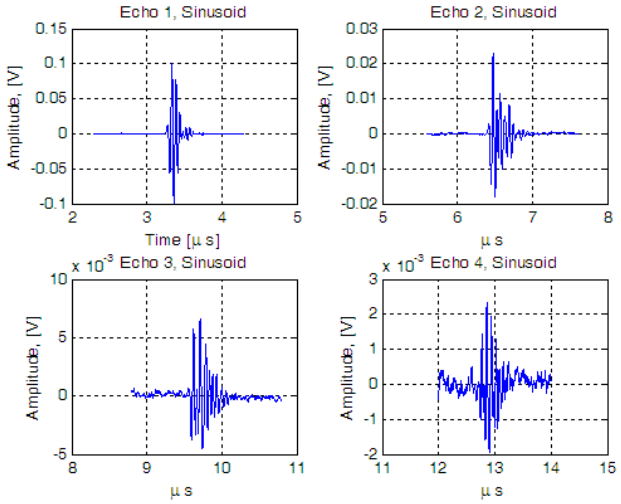

Figure 2: The echoes obtained with optimal positioning, element 1, sinusoidal excitation.

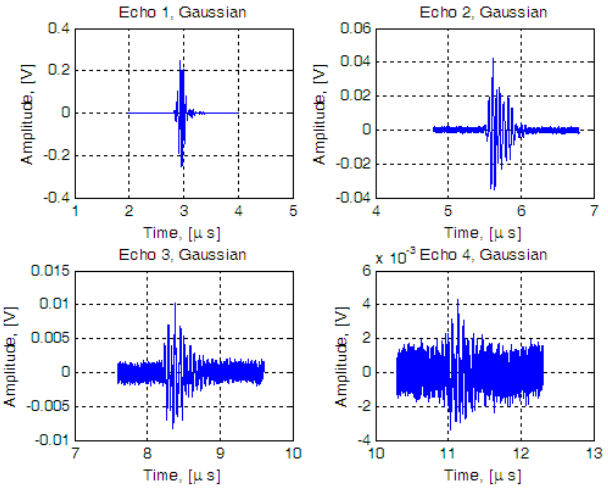

Figure 3: The echoes obtained with optimal positioning, element 2, Gaussian excitation.

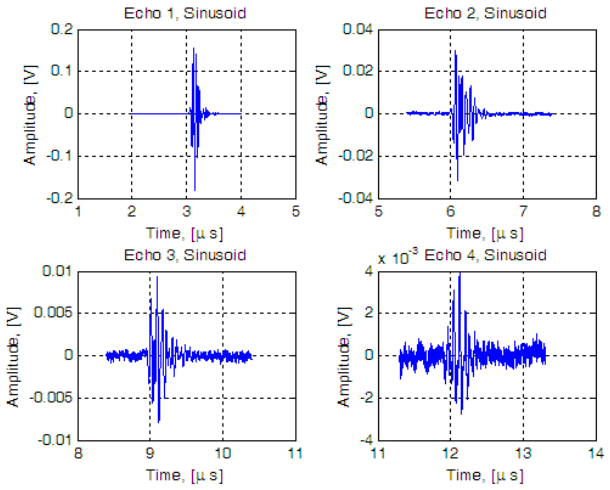

Figure 4: The echoes obtained with optimal positioning, element 2, sinusoidal excitation.